Computational Materials Science 164 (2019) 205–217

Contents lists available at ScienceDirect

Computational Materials Science

journal homepage: www.elsevier.com/locate/commatsci

Editor's Choice

Topological analysis of $CeMIn_5$ (M = Co, Rh) electron charge densities

M. Yazdani-Kachoei, S. Jalali-Asadabadi*, Negar Arianmehr

Department of Physics, Faculty of Sciences, University of Isfahan (UI), Hezar Gerib Avenue, Isfahan 81746-73441, Iran

ARTICLE INFO

Keywords:
Density functional theory
Full-potential APW + lo
Ce-based compounds
Bader's topological theory
CRITIC2

ABSTRACT

Recently, $CeRhIn_5$ and $CeCoIn_5$ with very different behaviors at ambient pressure were experimentally measured to exhibit comparable properties after applying pressure or doping impurity. Here, we study the electron charge densities (ECDs) of these compounds from topological point of view for the first time using the combination of DFT and quantum theory of atoms in molecules (DFT + QTAIM). We also investigate the electronic structures of these compounds including DOSs, band structures and electron charge densities (ECDs). The effects of applying pressure and degree of 4f-Ce electrons localization on properties of these compounds are also investigated, here. The DFT + QTAIM results in accordance with experiments reveal that at zero pressure these compounds have different TECD features and the features of $CeRhIn_5$ can become similar to those of $CeCoIn_5$, if in addition to applying pressure on $CeRhIn_5$ the degree of 4f-electron localization is also properly reduced. Our results also confirm that chemical pressure by Sn doping in $CeRhIn_5$ can make the features of its TECD somewhat similar to the pure $CeCoIn_5$.

1. Introduction

Isostructural $CeMIn_5$ compounds, where M is a transition metal have attracted considerable attentions recently due to showing a variety of interesting phenomena such as heavy-fermions [1–3], antiferromagnetism [4], and unconventional superconductivity [5–8], taking the roles of their quasi-2-dimensionality [9] in these phenomena into account in some cases. These attractive evidences have been found sensitive to and variable by the M-atoms [10–15]. At ambient pressure, for M = Co & Ir the case is an unconventional superconductor [10,11], while for M = Rh the case is an antiferromagnetic compound [13,16]. Electronic structures including densities of states (DOSs), band structures, electron charge densities (ECDs), and Fermi surfaces [17–23], along with magnetic [4,16,19,24,25], structural [26–28], and optical [14,15] properties as well as hyperfine interactions [29,19,30,31] have been theoretically and experimentally studied for these compounds. In this work, we perform topological analysis of electron charge density (TECD) for $CeRhIn_5$ and $CeCoIn_5$ as a first time and successfully extract consistent results with experiments. Although the TECD has been successfully used for a variety of materials to quantitatively study the nature of their bonds [32–34], it has not been applied on these technologically and fundamentally important materials yet. Our calculations were performed using a combination of DFT and Bader's topological theory of molecular structure, i.e., quantum theory of atoms in molecules (QTAIM) [35,36]. We also investigate the structural properties as well as DOSs, band structures and ECDs of these compounds. Comparison of experimental and DFT-based theoretical hyperfine interaction results in previous studies [29,19] reveals the high ability and success of DFT in describing the ECDs of these compounds. Previous theoretical calculations, in agreement with the experimental observations [37,38], have revealed that the degrees of 4f-electrons localizations are different in these compounds [39]. Thus, we perform our calculations taking both high and low 4f-localization regimes into account for these compounds. Based on our results, 4f-electrons are more localized in $CeRhIn_5$ than in $CeCoIn_5$, in agreement with previous studies [37–39].

In this theoretical study, we rely on the following two reliable and interesting experimental observations. The first observation is that at ambient pressure $CeRhIn_5$ is an AFM compound, whereas $CeCoIn_5$ is a superconductor (SC) with the highest $T_c \simeq 2.3$ K and does not order magnetically [13,11,10,12,14]. Mena and coworkers, consistent with this observation [13,11,10,12] have shown that optical properties of $CeCoIn_5$ are different from those of $CeRhIn_5$ [14]. The second observation [8,16,13] is that $CeRhIn_5$ becomes superconductor and behaves like $CeCoIn_5$ at critical pressure $P_c \simeq 2.3$ GPa with maximum $T_c \simeq 2.1$ K which is close but not identical to the T_c of $CeCoIn_5$ at ambient pressure. Shishido et al. [37,38], consistent with the latter observation [8,16,13], have experimentally verified that the 4f-electrons are more localized in $CeRhIn_5$ than in $CeCoIn_5$ and the increase in pressure applied on $CeRhIn_5$ compound is accompanied by the

* Corresponding author.
E-mail addresses: saeid.jalali.asadabadi@gmail.com, sjalali@sci.ui.ac.ir (S. Jalali-Asadabadi).

https://doi.org/10.1016/j.commatsci.2019.03.041
Received 4 June 2018; Received in revised form 22 February 2019; Accepted 23 March 2019

reduction of 4f-electrons localization which forces $CeRhIn_5$ to behave like $CeCoIn_5$. Our results show that the number and types of critical points (CPs) of ECD of $CeCoIn_5$ compound in the edges of (0 0 1)-plane differ from those of $CeRhIn_5$ compound at ambient pressure. Furthermore, the CPs features of $CeRhIn_5$ substantially differ from those of $CeCoIn_5$ specifically in (0 0 1)-plane. For instance, the bond CP existing in the (0 0 1)-plane of $CeCoIn_5$ has higher ρ, $\nabla^2\rho$, and stability with respect to that of $CeRhIn_5$. Thus, in accordance with the first experimental observations, our results also confirm that $CeRhIn_5$ and $CeCoIn_5$ compounds have different ECDs at zero pressure due to the different features of their TECDs. Regarding the second experimental observation, we investigate the changes of the TECD features in responding to the applied hydrostatic and chemical pressures on these materials. In accordance with experimental observations [8,16,13], our results also corroborate that applying pressure on $CeRhIn_5$ can cause the features of its TECD to become very similar to those of the $CeCoIn_5$ in (0 0 1)-plane provided that the compression is accompanied simultaneously by the reduction of the 4f-electron localization. For reducing the 4f-localization, we have used the band-like local density approximation (LDA) with the highest itinerant character among the other exchange-correlation functionals, e.g., localized hybrid functionals. As our recent calculations [40] show, only one exchange-correlation functional cannot be used for strongly correlated sytems in all of the pressure range, and in this case for each pressure range a suitable functional should be selected.

Furthermore, recently it has been experimentally reported that the P_c of $CeRhIn_5$ and T_c of $CeCoIn_5$ can be decreased by Sn doping [8,41,17,16,42,43]. This motivated us to study the effects of Sn doping on the electron density of these compounds, as well. In analogy to the hydrostatic pressure, our results show that chemical pressure by Sn doping can also make the electron density of $CeRhIn_5$ somewhat similar to that of $CeCoIn_5$ from topological point of view, but not as much as the hydrostatic pressure accompanied by reducing the degree of 4f-electrons localization. In agreement with experiments [8,41,17,16,42,43], it is shown that Sn doping in these compounds can play a dual role depending on its hosts.

2. Computational details

In this paper, the electronic structure part of the calculations is performed using the density functional theory (DFT) [44,45] employing the full potential augmented plane waves plus local orbitals (FP-APW + lo) method [46,47] as implemented in the WIEN2k code [48], in the presence of spin-orbit coupling (SOC) and spin polarization as well as orbital polarization. The $CeRhIn_5$ compound is in the AFM phase at zero pressure, while the $CeCoIn_5$ does not order magnetically [14]. So we performed the calculations in the non magnetic (NM) phase for $CeCoIn_5$ and in the AFM phase for $CeRhIn_5$. The k-space integration is done utilizing 270 special k-points in the irreducible wedge of the first Brillouin zone corresponding to 18 × 18 × 11 Monkhorst-Pack scheme [49] for the Co case. A 1 × 2 × 1 supercell is used for $CeRhIn_5$ case as well as doping Sn impurity into the compounds, and the mesh is reduced to 18 × 9 × 11 for this supercell. The $R_{MT}K_{MAX}$ is optimized to 8 for expanding the wave functions in terms of plane waves inside the interstitial region, while inside the muffin-tin spheres the cutoff parameter $l_{max} = 10$ is used for the expansion of wave functions in terms of lattice harmonics. The periodic charge density and potential are Fourier expanded up to $G_{max} = 12$. In addition to LDA and PBE-GGA, the hybrid functional B3PW91 [50,51] and GGA + U [52] approach with $U_{eff} = 6$ eV [20] are employed to treat the exchange–correlation term. The general form of the hybrid functional is:

$$E_{xc}^{\text{hybrid}} = E_{xc}^{\text{SL}} + \alpha(E_x^{\text{HF}} - E_x^{\text{SL}}), \tag{1}$$

where E_{xc}^{hybrid} and E_{xc}^{SL} are exchange–correlation energies of the hybrid and semilocal functionals, respectively. The α parameter determines the portion of Hartree-Fock (E_x^{HF}) and semilocal (E_x^{SL}) exchange energy. The B3PW91 functional is:

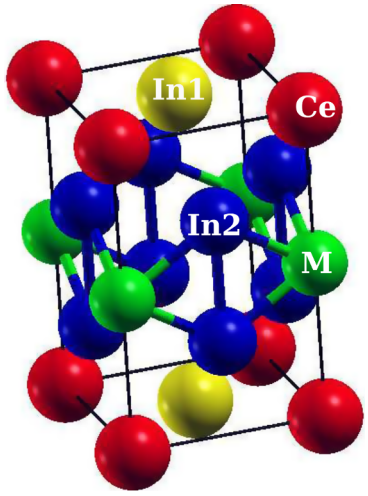

Fig. 1. $CeMIn_5$ structure.

$$E_{xc}^{B3PW91} = (1-\alpha)E_{xc}^{\text{LSDA}} + \alpha E_x^{\text{HF}} + \beta\Delta E_x^{\text{B88}} + E_c^{\text{LSDA}} + \gamma\Delta E_c^{\text{PW91}}, \tag{2}$$

where ΔE_x^{B88} is the Becke's 1988 gradient correction to the exchange functional [53] and ΔE_c^{PW91} is the Perdew-Wang gradient correction for the correlation functional [54]. Becke optimized the coefficients to $\alpha = 0.2$, $\beta = 0.72$ and $\gamma = 0.81$ [55]. However, we used several values for the α parameter to seek better optimization for our cases.

The $CeMIn_5$ compounds crystallize in tetragonal $HoCoGa_5$ structure [26–28] (P4/mmm space group number 123) with four non-equivalent atomic positions. These atomic positions are Ce: (0, 0, 0), M: (0, 0, 0.5), In1: (0.5, 0.5, 0) and In2: (0, 0.5, z) as shown in Fig. 1. In the Sn doped cases the non-equivalent atomic positions are increased to 7 as shown in Fig. 2. The experimental lattice parameters reported in Table 1 are used as input parameters [27,28]. Full-relaxation is applied to reduce the total forces on all atoms to values smaller than 0.5 mRy/bohr. The internal parameters (z) for these compounds along with experimental results [27,28] are calculated and reported in Table 1. As shown in this table, the calculated z's are in good agreement with the experimental results.

The topological analysis part of the work is carried out using the CRITIC2 code [56,57] which is based on the quantum theory of atoms in molecules (QTAIM) [35,36]. Electron charge density (ECD) distribution, $\rho(\mathbf{r})$, is a physical quantity which is defined as a scalar field over a three-dimensional space. Topological properties of this scalar

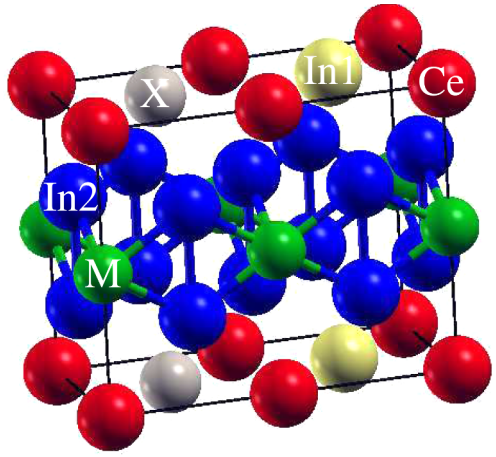

Fig. 2. A 1 × 2 × 1 supercell used for doping Sn impurity into the $CeMIn_5$ structure as well as AFM calculations. For doping Sn impurity (AFM calculations) X = Sn (X = In1).

Table 1
Calculated optimized volumes and bulk moduli (B_0's) of $CeMIn_5$ (M = Co, Rh) compounds within various exchange-correlation functionals along with the experimental data (Exp.'s) for comparison. The calculations of $CeRhIn_5$ and $CeCoIn_5$ are carried out in antiferromagnetic (AFM) and non magnetic (NM) phases, respectively. The theoretical internal parameter of In2, i.e., z-In2, for both cases along with corresponding experimental data are also presented.

	$CeRhIn_5$		$CeCoIn_5$	
	Vol_{opt}	B_0	Vol_{opt}	B_0
LDA	154.48	92.90	149.36	90.55
PBE-GGA	168.71	71.73	162.78	67.55
GGA + U (U_{eff} = 6 eV)	170.84	68.25	163.39	66.26
B3PW91-α = 0.05	163.55	76.72	157.33	75.99
B3PW91-α = 0.10	164.22	74.82	157.34	75.90
B3PW91-α = 0.20	165.05	75.01	156.66	77.91
B3PW91-α = 0.30	165.62	75.30	156.44	77.72
Exp. [27,28,58]	163.50	78.4	160.68	78.2

z-In2

	$CeRhIn_5$	$CeCoIn_5$
B3PW91-α = 0.20		0.3047
B3PW91-α = 0.05	0.3109	
Exp. [27,28]	0.3094	0.3059

field can be described by determination of number, kind and position of its critical points (CPs). Gradient of $\rho(\mathbf{r})$, $\nabla\rho(\mathbf{r})$, is zero in CPs. Hence, these points determine the extrema positions of $\rho(\mathbf{r})$. The kind of these extrema, i.e., maxima, minima or saddle points, is determined by the curvature of $\rho(\mathbf{r})$ at these CPs. The $\rho(\mathbf{r})$ curvature is determined by using the Hessian matrix of $\rho(\mathbf{r})$ which has nine components of the form $\partial^2\rho/\partial x_i\partial x_j$, within an arbitrary axes system. By diagonalizing this matrix, three eigenvalues (λ_1, λ_2, λ_3) and three eigenvectors (X_1, X_2, X_3) are obtained, where $\lambda_1 = \frac{\partial^2\rho}{\partial X_1^2}$, $\lambda_2 = \frac{\partial^2\rho}{\partial X_2^2}$, and $\lambda_3 = \frac{\partial^2\rho}{\partial X_3^2}$. The ($X_1$, X_2, X_3) coordinate axes are defined as the principal axes of curvatures, where the Hessian matrix of $\rho(\mathbf{r})$ is diagonal there. Each critical point can be labeled by the two numbers (ω, σ), where ω determines the number of none-zero eigenvalues of $\rho(\mathbf{r})$ curvature, and σ is the algebraic sum of the signs of the eigenvalues at a CP. For ω = 3, four possible σ's, i.e., $\sigma = -3, -1, +1, +3$, can be existed. For the (3, −3) critical point $\lambda_1, \lambda_2, \lambda_3 < 0$. This shows a local maximum in $\rho(\mathbf{r})$ at this CP and is called a nuclear critical point (NCP or simply n) [35]. The (3, −1) [(3, +1)] critical point has two negative [positive] and one positive [negative] eigenvalues. At (3, −1) [(3, +1)] point, the $\rho(\mathbf{r})$ has a maximum [minimum] in the plane defined by the eigenvectors related to two negative [positive] eigenvalues and a minimum [maximum] along the third eigenvector. The (3, −1) point is founded between two nuclei which are linked by the chemical bond [35]. Thus, it is defined as a bond critical point (BCP or b) [35]. The (3, +1) is defined as a ring critical point (RCP or r). For the (3, +3) critical point, we have $\lambda_1, \lambda_2, \lambda_3 > 0$. This point shows a local minimum for $\rho(\mathbf{r})$ and is called as a cage critical point (CCP or c) [35].

3. Structural properties

In order to select an accurate scheme for describing the compounds under study, we investigate the structural properties of heavy fermions $CeMIn_5$ (M = Co, Rh) within both low and high localized 4f-Ce electrons regimes. To this end, the volumes and bulk moduli of the compounds are calculated by various exchange-correlation functionals. In order to obtain the structural properties, the total energies of the unit cells are calculated as a function of their volumes and fitting the data with the Birch-Murnaghan isothermal equation of state [59]. The results together with the available experimental data [27,28,58] for comparison are tabulated in Table 1 and represented in Fig. 3. The results show that neither LDA nor PBE-GGA functional is successful enough for predicting structural properties of $CeCoIn_5$ and $CeRhIn_5$. The volumes are predicted by LDA (PBE-GGA) functional to be smaller (larger) than the experimental results for both $CeRhIn_5$ and $CeCoIn_5$ cases. Thus, from the latter statement one can conclude that the volumes predicted by PBE-GGA must be also larger than those predicted by the low localized LDA results, as can be authenticated by the results given in Table 1 and Fig. 3. However, the situation is completely reversed for the bulk moduli of the compounds; the bulk moduli are predicted by LDA (PBE-GGA) functional to be larger (smaller) than the experimental results [58]. Thus, in contrast to the volumes, the bulk moduli are predicted by PBE-GGA to be lower than those predicted by LDA for both cases, see Table 1. Although the PBE-GGA predicts the volume of $CeCoIn_5$ in good agreement with experiment, it predicts the bulk modulus of this case very far from the experiment. The Table 1 shows that adding the U parameter to this functional makes the results worse. The volumes (bulk moduli) are predicted by the GGA + U with U_{eff} = 6 eV to be larger (lower) and as a result worse than those predicted by the standard PBE-GGA. Therefore, GGA + U also seems not to be very suitable for our cases. In order to improve the results, we use the hybrid functionals B3PW91-α = 0.05, B3PW91-α = 0.10, B3PW91-

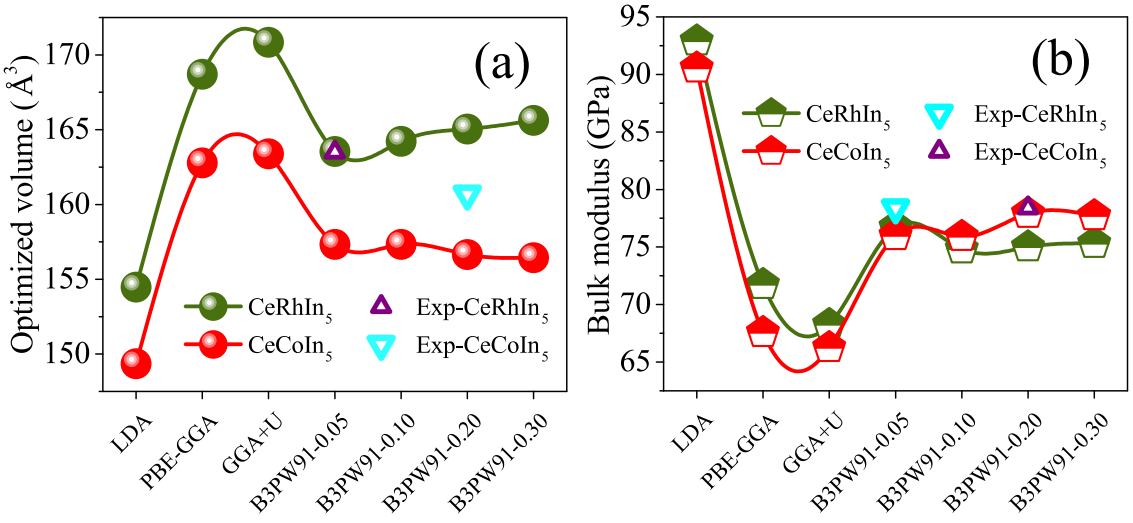

Fig. 3. (a) Optimized volume in Å^3, and (b) bulk modulus (B_0) in GPa versus different exchange-correlation functionals for $CeRhIn_5$ and $CeCohIn_5$ compounds including experimental data [27,28,58] for comparision.

$\alpha = 0.2$ and B3PW91-$\alpha = 0.3$, as the other alternatives. The degree of localization using these functionals is tuned by the value of α parameter. Based on the recent studies [60–63,40], the success of hybrid functionals depends on the value of α parameter. The results show that B3PW91-$\alpha = 0.05$ functional predicts larger volume(smaller bulk modulus) compared to LDA for both cases and thereby improves the LDA results. According to our results, volume and bulk modulus of $CeRhIn_5$ are well predicted by B3PW91-$\alpha = 0.05$ functional compared to the other used functionals. Furthermore, the B3PW91-$\alpha = 0.05$ functional also predicts the internal parameter, i.e., $z - In2$ of $CeRhIn_5$ in good agreement with experiments [27,28], see Table 1. To improve the B3PW91-$\alpha = 0.05$ results, we increase its α parameter to 0.10, 0.20 and 0.30. As Table 1 reveals, the structural properties calculated by B3PW91 with $\alpha = 0.20$, 0.10 & 0.30 are made worse compared to the experimental data than those of B3PW91-$\alpha = 0.05$. Therefore, among the listed functionals in Table 1, B3PW91-$\alpha = 0.05$ can be considered as the best functional for describing the structural properties of $CeRhIn_5$ in agreement with the experimental data. For the Co case the B3PW91-$\alpha = 0.20$ leads to the best result for the bulk modulus of Co case compared the other considered functionls, however, this functional cannot predict the volume of Co case better than the PBE-GGA, GGA + U with $U_{eff} = 6$ eV and B3PW91-$\alpha = 0.05$, &0.10. But, it seems that the B3PW91-$\alpha = 0.20$ leads to the best results for structural properties of $CeCoIn_5$ among the considered functionals, if we consider both volume and bulk modulus, simultaneously.

4. Electronic structure

In this section, we calculate the electronic structures including densities of states (DOSs), band structures, and electronic charge densities (ECDs) at P= 0 and 4.5 GPa. We also perform the electronic structure calculations at high, intermediate, and low degrees of localization of the 4f-Ce electrons by employing the high localized B3PW91-$\alpha = 0.2$, moderate localized B3PW91-$\alpha = 0.05$ and low localized LDA exchange–correlation functionals, respectively. As we discussed in Section 2, the calculations of $CeRhIn_5$ ($CeCoIn_5$) are done in AFM (NM) phase.

4.1. Density of states (DOS)

We begin the discussion by analyzing the DOSs of $CeCoIn_5$ and $CeRhIn_5$ compounds as calculated by the B3PW91-$\alpha = 0.20$ at zero and P = 4.5 GPa pressures. The DOSs at Fermi level, DOSs(E_F), are represented in Table 2. The results show that contributions of Ce atoms in the total DOS(E_F) are larger than the other atoms for both of the compounds at both P = 0 and 4.5 GPa pressures using B3PW91-$\alpha = 0.20$, see Table 2. We also observe that all the DOSs(E_F) except those of In in Co case slightly decrease by imposing pressure for both cases using B3PW91-$\alpha = 0.20$, see the first and second rows of Table 2. The calculated total DOSs, as well as partial 4f-Ce and d-M (M = Co, Rh) DOSs of the cases under study at zero (4.5 GPa) pressure using B3PW91-$\alpha = 0.2$ are displayed in Fig. 4(a_{11}) (Fig. 4(a_{12}) for $CeCoIn_5$ and in Fig. 4(b_{11}) (Fig. 4(b_{12}) for $CeRhIn_5$. Our results show that the total DOSs of both compounds can be predominantly characterized by the 4f-Ce DOSs in the vicinity of their Fermi levels (E_F's); the total DOSs are mainly formed by the 4f-Ce DOSs nearby the E_F's. The first row of Fig. 4 reveals that the 4f-Ce DOSs cross E_F and most of them are located above the E_F using B3PW91-$\alpha = 0.20$ functional at both zero and 4.5 GPa pressures. Actually, the occupied 4f-Ce DOSs below the E_F are shifted towards higher unoccupied energies above the E_F by applying the high localized B3PW91-$\alpha = 0.20$ functional compared to the other less localized functionals; compare the first row with the second or third row of Fig. 4. Such a shift is in agreement with the results obtained from LDA + U calculations performed by M. Gamża et al. for $CeMIn_5$ [20]. Our results show that the total, d-M (M = Co, Rh), and 4f-Ce DOSs cannot be drastically changed by applying pressure for both of the compounds, compare the first column (a_{i1}) with the corresponding second column (a_{i2}) of Fig. 4 and/or the third column (b_{i1}) with the corresponding fourth column (b_{i2}) of Fig. 4, for every $i = 1$ to 3. This result seems to be almost independent of the kind of our used exchange-correlation functionals, because it is obtained by three different exchange-correlation functionals, i.e., B3PW91-$\alpha = 0.20$, and B3PW91-$\alpha = 0.05$, as well as LDA, as shown in the first, second and third rows of Fig. 4. This shows that the pressure effects on DOSs of $CeMIn_5$ (M = Co, Rh) are theoretically predicted by DFT to be almost negligible, if only a fixed functional is used for every pressure which is not always occurred in nature or experimentally permitted. This result is similar to the recent result reported for $CeIn_3$ compound [40]. In contrast, the total and 4f-Ce DOSs can be drastically changed by changing the degree of 4f-Ce localization for both of the compounds, compare the first (x_{1j}), second (x_{2j}), and third (x_{3j}) rows of Fig. 4 with each other correspondingly, for every x= a, b, and $j = 1, 2$. The results reveal that decreasing the degree of 4f-Ce localization causes the 4f-Ce DOS as well as total DOS to pile up around the Fermi level, compare Fig. 4(a_{11}) with Fig. 4(a_{31}) or more generally the first row with the corresponding second and third rows of Fig. 4. This result is consistent with the recent observation [40] for $CeIn_3$. Our results in agreement with the results reported by M. Gamża et al. show that decreasing the degree of 4f-Ce localization also increases the Ce and total DOSs(E_F) for both cases, see Table 2.

4.2. Band structure

Band structures of the compounds using B3PW91-$\alpha = 0.20$, B3PW91-$\alpha = 0.05$, and LDA at P = 0 & 4.5 GPa are displayed in Figs. 5(x_{ij}) for both compounds, where x= a, b, $i = 1, 2, 3$, and $j = 1, 2$. Note that the figure only shows those bands cross the Fermi level. In this figure similar to Fig. 4, the symbol x stands for the kinds of the compounds, i.e., x= a refers to $CeCoIn_5$ and x= b refers to $CeRhIn_5$. Furthermore, the index i stands for the types of the exchange–correlation functionals, i.e., $i = 1$ refers to B3PW91-$\alpha = 0.20$, $i = 2$ refers to B3PW91-$\alpha = 0.05$, and $i = 3$ refers to LDA, while the index j stands for the pressure values, i.e., $j = 1$ and 2 refer to P = 0 and 4.5 GPa,

Table 2
Total DOSs at the Fermi level DOS(E_F) (States/eV) along with the atomic contributions within various exchange- correlation functionals at P = 0 and 4.5 GPa for $CeCoIn_5$ in non magnetic (NM) phase and $CeRhIn_5$ in antiferromagnetic (AFM) phase.

		$CeCoIn_5$					$CeRhIn_5$				
XCF	P (GPa)	Total	Ce	Co	In1	In2	Total	Ce	Rh	In1	In2
B3PW91-$\alpha = 0.20$	0	3.2512	1.9097	0.3948	0.0418	0.1751	6.0127	1.4213	0.8476	0.3999	0.5684
	4.5	3.1373	1.8166	0.3756	0.0428	0.1872	5.3574	1.3031	0.7222	0.3617	0.5307
B3PW91-$\alpha = 0.05$	0	4.6015	2.6176	0.5476	0.0825	0.2620	8.4616	3.9618	0.7984	0.3982	0.5146
	4.5	4.5142	2.6078	0.5101	0.0856	0.2678	7.8506	3.7980	0.6876	0.3621	0.4869
LDA	0	5.1944	3.1404	0.5443	0.0899	0.2711	17.7962	11.4952	0.8522	0.5465	0.7095
	4.5	4.8018	2.8602	0.5090	0.0901	0.2735	17.7675	10.6317	0.8178	0.5632	0.7384

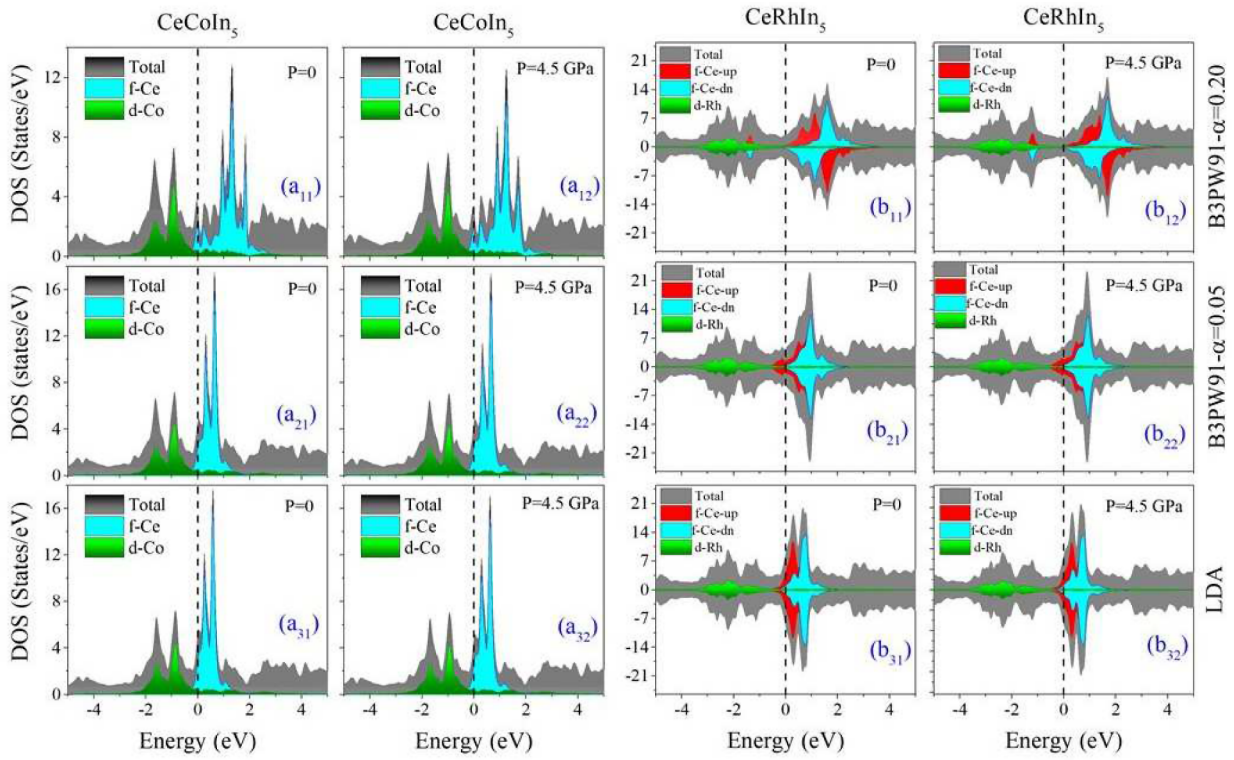

Fig. 4. The calculated total and partial 4f-Ce, as well as d-M DOSs of $CeMIn_5$ (M = Co, Rh) compounds at zero and P = 4.5 GPa pressures using B3PW91-α = 0.20, B3PW91-α = 0.05, and LDA. The calculations of $CeRhIn_5$ and $CeCoIn_5$ are carried out in antiferromagnetic (AFM) and non magnetic (NM) phases, respectively. Here, the character x stands for the names of the compounds, i.e., x= a refers to $CeCoIn_5$ and x= b refers to $CeRhIn_5$. The index i stands for the types of the exchange–correlation functionals so that i = 1 refers to B3PW91-α = 0.20, i = 2 refers to B3PW91-α = 0.05, and i = 3 refers to LDA. The index j stands for the pressure values so that j = 1 refers to P = 0 and j = 2 refers to P = 4.5 GPa. Fermi level is set to zero.

respectively. The partial 4f-Ce states are also displayed in the band structure figures; the larger the thicknesses of the bands, the more contributions the 4f-Ce states have in the vicinity of Fermi level. Comparing Figs. 5(x_{i1}) with Figs. 5(x_{i2}) for x= a, b, and i = 1 to 3 reveals that the effects of pressure on the band structures are almost negligible for both compounds using LDA, B3PW91-α = 0.05, and B3PW91-α = 0.20.

The Figs. 5(x_{1j}) for x= a, b, and j = 1, 2 calculated by B3PW91-α = 0.20 show that six (three) bands cross the Fermi level at zero and 4.5 GPa pressures in $CeRhIn_5$ ($CeCoIn_5$) compound. Thus, B3PW91-α = 0.20 predicts that the number of bands crossing the Fermi level is not changed by applying this pressure. Let us explore more details about the bands. To this end, some of the important characteristics of these bands, including maximum energy (E_{max}), minimum energy (E_{min}), band width (Width), and occupation number (Occup), are tabulated in Table 3 at P = 0 and 4.5 GPa for both compounds using LDA, B3PW91-α = 0.05, and B3PW91-α = 0.20. Note that the E_{min} and E_{max} are measured in eV with respect to the Fermi energy so that a negative (positive) energy lies below (above) the Fermi energy. This table shows that the characteristics of the bands are not significantly influenced and the number of bands crossing the Fermi level is not changed by pressure. These results are independent of the compounds and functionals used, see Table 3. In contrast, the characteristics of the bands crossing the Fermi level are changed by the degree of 4f-Ce localization, i.e., by the functionals used. The latter result is independent of the compounds under question and the pressures applied here, see Table 3. For the $CeRhIn_5$, the number of bands crossing the Fermi level are also changed by the degree of 4f-Ce localization, while this is not the case for $CeCoIn_5$. To be more specific, decreasing the degree of 4f-Ce localization from high degree (using B3PW91-α = 0.20) to intermediate degree (using B3PW91-α = 0.05) and/or low degree (using LDA) causes the γ6, as one of the bands which crosses the Fermi level in Rh case, to be located completely above the Fermi level. As Table 3 shows for $CeRhIn_5$ at both P = 0 and 4.5 GPa the occupation number of γ6 is less than one and its E_{min} (E_{max}) is negative (positive) using B3PW91-α = 0.20 & 0.05, while its occupation number is zero and its E_{min} is positive using LDA. Hence, five bands cross the Fermi level using LDA functional, whereas six bands cross the Fermi level using B3PW91-α = 0.20 & 0.05 in $CeRhIn_5$ compound. Similar result is also reported for $CeIn_3$ compound [40]. For the Co case three bands cross the Fermi level within three considered functionals at both P = 0 and 4.5 GPa pressures. Thus, the number of the bands crossing the Fermi level are not changed by the degree of 4f-Ce localization as well as pressure for Co case.

4.3. Electron charge density (ECD)

The ECDs of these compounds calculated by B3PW91-α = 0.20, B3PW91-α = 0.05, and LDA at P = 0, and 4.5 GPa pressures are presented in Fig. 6 for (0 0 1)-plane and in Fig. 7 for (100)-plane. In these figures, the definitions of a_{ij}, b_{ij}, and their indices i and j are analogous to those of Figs. 4 and 5 and thereby would not be repeated here.

The Figs. 6 and 7 reveal that the ECDs are mainly and almost spherically distributed nearby the atomic positions in the unit cells of the compounds and gradually decreased by increasing the distances from the atomic positions so that only a small amount of ECDs can be found outside these spheres-like charge distributions shown in these figures. The Fig. 6 reveals that there are minima of ECDs (with light blue color) in the middle regions between the Ce–Ce bonds compared to the other regions, while this figure shows that there are higher ECDs (with green color) in the middle regions between the Ce-In1 bonds in the (0 0 1)-plane for both cases with all of the considered pressures and functionals. The same result can be also observed for the Ce-Ce bonds in the (1 0 0)-plane, as shown in Fig. 7; see the ECD minima (the light blue

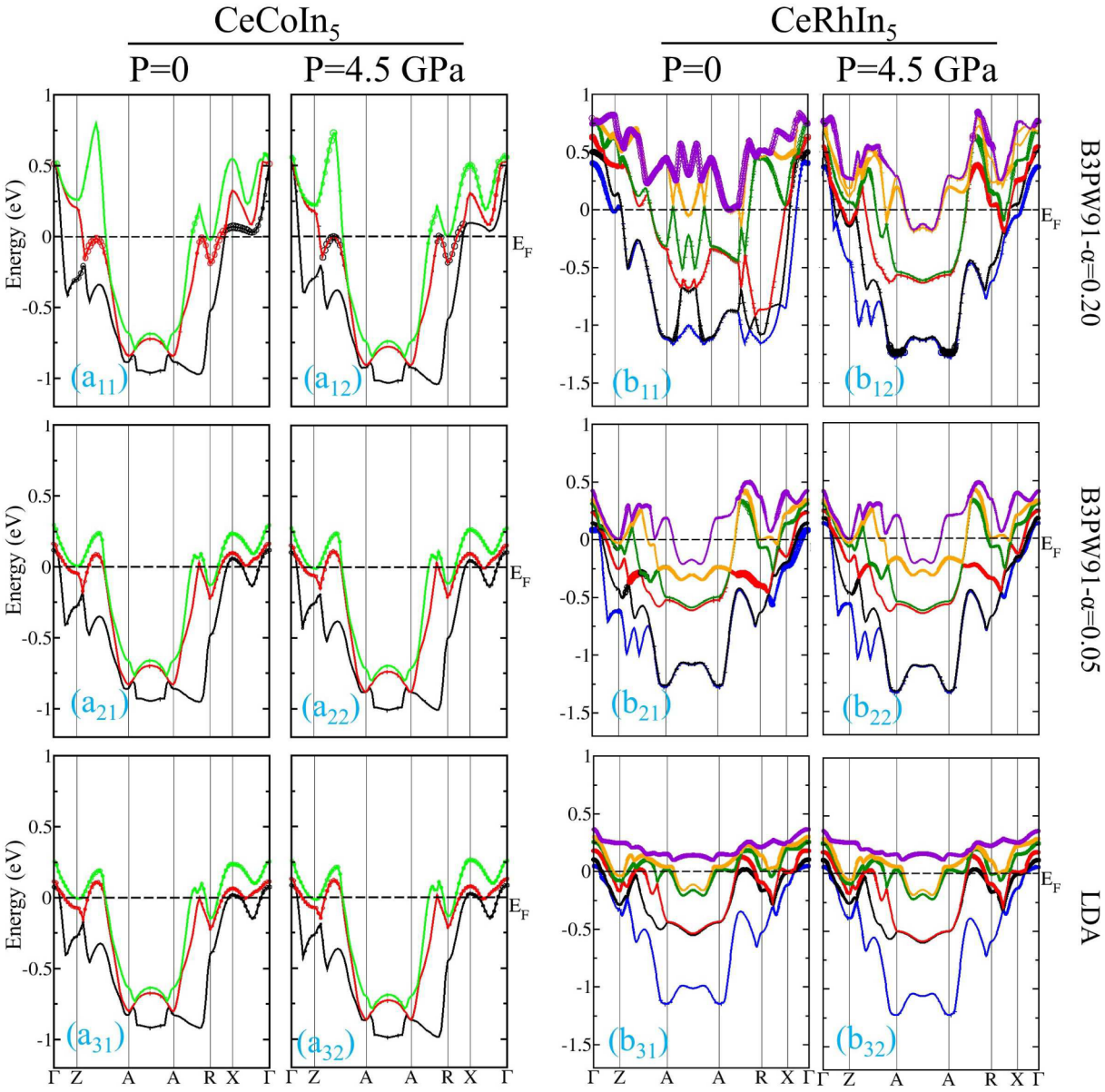

Fig. 5. The calculated band structures of $CeCoIn_5$ in non magnetic (NM) phase and $CeRhIn_5$ in antiferromagnetic (AFM) phase compounds at zero and P = 4.5 GPa pressures using B3PW91-α = 0.20, B3PW91-α = 0.05, and LDA. Here, the character x stands for the names of the compounds, i.e., x= a refers to $CeCoIn_5$ and x=b refers to $CeRhIn_5$. The index i stands for the types of the exchange–correlation functionals so that i = 1 refers to B3PW91-α = 0.20, i = 2 refers to B3PW91-α = 0.05, and i = 3 refers to LDA. The index j stands for the pressure values so that j = 1 refers to P = 0 and j = 2 refers to P = 4.5 GPa. Fermi level is set to zero. Each band is characterized by special color. The line width of bands reveals the 4f-Ce states portion in each band. In this figure only those bands crossing the Fermi level are shown.

color) between Ce-Ce bonds. The comparison of Figs. 6 and 7 shows that the electronic charges are slightly more accumulated in the middle regions between M (M = Co, Rh) and In2 atoms in (1 0 0)-plane than the other regions in both (1 0 0)- and (0 0 1)-planes of the compounds; see red color having higher scale between In2 and M atoms in (1 0 0)-plane. This result is consistent with the previous result reported by Gamża et al. [20] on the ECD analysis of $CeMIn_5$. In other words, Fig. 7 shows some ECD maxima (with red color) in the middle regions between M-In2 bonds. This implies that the M-In2 bonds are even stronger than Ce-In1 bonds; the scale of red color in Fig. 7 is larger than that of green color in Fig. 6. It can be also clearly seen from Fig. 7 that M and Ce atoms are weakly bonded to each other in (1 0 0)-plane for both M=Co and Rh; see the light blue color having low scale in the regions between Co–Ce and Rh-Ce bonds. Thus, we expect to see some minima in the ECDs between Ce and M atoms in (1 0 0)-plane the same as Ce–Ce in (0 0 1)-plane. Fig. 6 shows that Ce–In1 bonds are connected (by green color) more strongly than Ce–Ce bonds (by blue color) in (0 0 1)-plane. This can be considered as a surface that curves up in one direction, while it curves down in the other different direction. In both directions, the derivatives become zero without showing a local extremum (minimum or maximum) on both directions, resembling a riding saddle critical point in the domain of the ECDs shown in Fig. 6; saddle point can be defined as a stationary point of a two-variables function where the partial derivatives of its orthogonal components vanish without having a local maximum or minimum on both orthogonal axes. The same behavior can be seen in Fig. 7 which shows that M-In2 bonds are connected (by red color) more strongly than Ce-Ce bonds (by blue color) in (1 0 0)-plane. Therefore, we expect to observe a saddle critical point in (1 0 0)-plane of these compounds, as well. We will systematically discuss the critical points of these compounds under various

Table 3
Maximum energy (E_{max}), minimum energy (E_{min}), band width (Width), and occupation number (Occup) of bands crossing the Fermi level in $CeRhIn_5$ in AFM phase and $CeCoIn_5$ in NM phase calculated using various functionals at P = 0 and 4.5 GPa. E_{max} and E_{min} are measured with respect to the Fermi level so that positive energies are located above the Fermi level while negative energies are located below the Fermi level.

		Band	E_{min} (eV)		E_{max} (eV)		Width (eV)		Occup	
			P = 0	P = 4.5 GPa	P = 0	P = 4.5 GPa	P = 0	P = 4.5 GPa	P = 0	P = 4.5 GPa
$CeCoIn_5$	B3PW91-α = 0.2	γ1	-0.9623	-1.0339	0.3794	0.3671	1.3417	1.4010	0.9718	0.9729
		γ2	-0.8225	-0.8893	0.4066	0.4330	1.2291	1.3222	0.7753	0.7667
		γ3	-0.7467	-0.8064	0.8087	0.7437	1.5555	1.5501	0.2529	0.2601
	B3PW91-α = 0.05	γ1	-0.9438	-1.0016	0.0998	0.0883	1.0436	1.0899	0.9913	0.9933
		γ2	-0.8071	-0.8610	0.1421	0.1376	0.9493	0.9986	0.7285	0.7220
		γ3	-0.7220	-0.7619	0.2645	0.2659	0.9865	1.0277	0.2803	0.2847
	LDA	γ1	-0.9100	-0.9787	0.0608	0.0697	0.9709	1.0484	0.9959	0.9954
		γ2	-0.7730	-0.8388	0.1107	0.1212	0.8837	0.9600	0.7207	0.7194
		γ3	-0.6857	-0.7430	0.2308	0.2540	0.9166	0.9970	0.2834	0.2853
		Band	E_{min} (eV)		E_{max} (eV)		Width (eV)		Occup	
			P = 0	P = 4.5 GPa	P = 0	P = 4.5 GPa	P = 0	P = 4.5 GPa	P = 0	P = 4.5 GPa
$CeRhIn_5$	B3PW91-α = 0.2	γ1	-1.2719	-1.3374	0.2904	0.3085	1.5623	1.6458	0.9743	0.9716
		γ2	-1.2273	-1.2359	0.3521	0.3572	1.5794	1.5931	0.9314	0.9138
		γ3	-1.0049	-1.0839	0.5377	0.5608	1.5426	1.6447	0.6153	0.6173
		γ4	-0.6730	-0.6879	0.5945	0.6809	1.2674	1.3688	0.4283	0.4452
		γ5	-0.1881	-0.1947	0.8045	0.8344	0.9926	1.0290	0.0501	0.0514
		γ6	-0.0448	-0.0415	0.8749	0.8945	0.9197	0.9360	0.0008	0.0007
	B3PW91-α = 0.05	γ1	-1.3077	-1.3705	0.1049	0.1512	1.4126	1.5217	0.9897	0.9885
		γ2	-1.2551	-1.3491	0.1785	0.1783	1.4336	1.5274	0.9756	0.9772
		γ3	-1.0392	-1.1230	0.2385	0.2317	1.2777	1.3547	0.9043	0.9075
		γ4	-0.7879	-0.8373	0.3641	0.3477	1.1520	1.1851	0.6641	0.6801
		γ5	-0.2967	-0.3015	0.4621	0.4452	0.7588	0.7467	0.4058	0.3960
		γ6	-0.1755	-0.1732	0.5344	0.5072	0.7099	0.6804	0.0606	0.0507
	LDA	γ1	-1.1938	-1.2813	0.0414	0.0507	1.2353	1.3321	0.9907	0.9893
		γ2	-0.9662	-1.0477	0.0960	0.1095	1.0622	1.1572	0.9444	0.9354
		γ3	-0.7510	-0.7991	0.1802	0.1844	0.9312	0.9835	0.7222	0.7251
		γ4	-0.2378	-0.2660	0.2567	0.2573	0.4945	0.5233	0.3004	0.3063
		γ5	-0.1399	-0.1582	0.2867	0.2906	0.4266	0.4488	0.0423	0.0446
		γ6	0.1124	0.1347	0.3516	0.3524	0.2392	0.2177	0.0000	0.0000

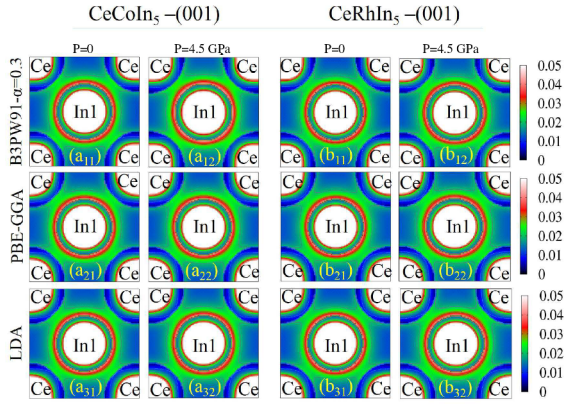

Fig. 6. Electronic charge densities (ECDs) for spin up calculated by B3PW91-α = 0.20, B3PW91-α = 0.05, and LDA at zero and 4.5 GPa pressures in (001)-plane for (a_{ij}) $CeCoIn_5$ in NMand (b_{ij}) $CeRhIn_5$ in AFM phase, where index *i* varies from 1 to 3 and index *j* varies from 1 to 2. For the definitions and physical meanings of these indices one would refer to the text or captions of Figs. 4 and 5.

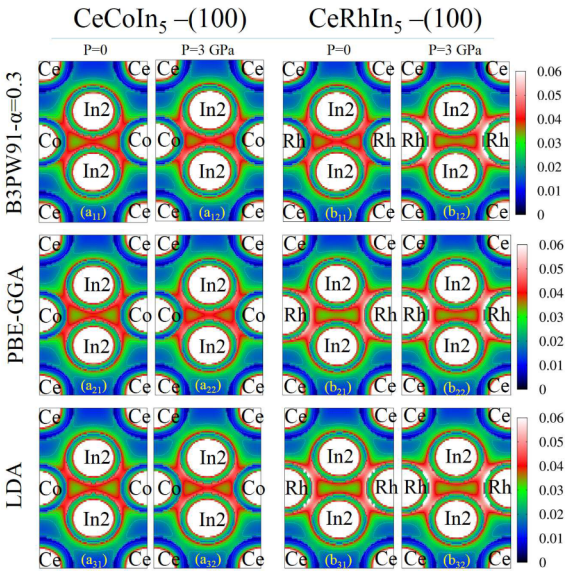

Fig. 7. Electronic charge densities (ECDs) for spin up, calculated by B3PW91-α = 0.20, B3PW91-α = 0.05, and LDA at zero and 4.5 GPa pressures in (100)-plane for (a_{ij}) $CeCoIn_5$ in NM and (b_{ij}) $CeRhIn_5$ in AFM phase, where index *i* varies from 1 to 3 and index *j* varies from 1 to 2, as defined in the text and captions of Figs. 4 and 5.

circumstances in subsequent section. Thus, let us back to the main point of this section. The ECDs are not remarkably affected by pressure or decreasing the degree of 4f-Ce localization, see Figs. 6 and 7. Thus, we aim to perform more elaborations by revisiting quantitatively the ECD results. To this end, we eventually perform a systematic topological analysis of ECDs in the following section.

Table 4
Number and types of non-equivalent CPs for $CeRhIn_5$ in antiferromagnetic (AFM) phase and $CeCoIn_5$ in nonmagnetic (NM) phase calculated within LDA and B3PW91-$\alpha = 0.05$, B3PW91-$\alpha = 0.20$ functionals at P = 0 and 4.5 GPa pressures. The numbers in parentheses represent the number of equivalent CPs.

	Pressure (GPa)	NCP	BCP	RCP	CCP
		B3PW91-$\alpha = 0.20$			
$CeCoIn_5$	0	4(7)	5(30)	4(36)	4(13)
	4.5	4(7)	5(30)	4(36)	4(13)
$CeRhIn_5$	0	8(14)	16(60)	15(76)	9(30)
	4.5	8(14)	16(60)	15(76)	9(30)
		B3PW91-$\alpha = 0.05$			
$CeCoIn_5$	0	4(7)	5(30)	4(36)	4(13)
	4.5	4(7)	5(30)	4(36)	4(13)
$CeRhIn_5$	0	8(14)	16(60)	15(76)	9(30)
	4.5	8(14)	16(60)	15(76)	9(30)
		LDA			
$CeCoIn_5$	0	4(7)	5(30)	4(36)	4(13)
	4.5	4(7)	5(30)	4(36)	4(13)
$CeRhIn_5$	0	8(14)	16(60)	12(72)	8(26)
	4.5	8(14)	16(60)	12(72)	8(26)

5. Topological analysis

CPs are obtained by $\nabla\rho(\mathbf{r}) = 0$ for the compounds under questions, and then the numbers of them are counted and their types, i.e, NCP, BCP, CCP, and RCP, are accordingly determined by the sings of $\lambda_i = \frac{\partial^2\rho}{\partial x_i^2}$ (for $i = 1$ to 3), as tabulated in Table 4. From this table it can be seen that the numbers of the CPs presented in this table satisfy the Morse condition [57], *viz.*, NCP − BCP + RCP − CCP = 0.

Furthermore, the numbers of non-equivalent and equivalent CPs in $CeRhIn_5$ are different from (more than) those of $CeCoIn_5$ within B3PW91-$\alpha = 0.20$. As the Table 4 shows the numbers of equivalent NCPs and BCPs in $CeRhIn_5$ are twice as many as $CeCoIn_5$. This is because we use a $2 \times 2 \times 2$ supercell for Rh-case. However, this is not the case for RCPs and CCPs; the numbers of RCPs and CCPs in $CeRhIn_5$ are not twice as many as $CeCoIn_5$. The CPs of these compounds calculated within B3PW91-$\alpha = 0.20$ are displayed for (0 0 1)-plane in the left panel, and for (1 0 0)-plane in the right panel of Fig. 8. From the left panel of Fig. 8, we observe one non-equivalent BCP (b1) between In1 and Ce, and one non-equivalent CCP (c1) between every two Ce atoms in the (0 0 1)-plane of the compounds. These CPs are consistent with the ECD results discussed in the previous section. For $CeRhIn_5$, in addition to the c1, there is also one RCP (r1) between the Ce atoms, see Fig. 8(f_{21}). For $CeCoIn_5$ ($CeRhIn_5$), the c1 (r1) is positioned at the middle of the line connecting the two Ce atoms and there is (are) one (two) equivalent c1 CCP(s). From the right panel of Fig. 8, except for the [1 0 0]-direction between Ce atoms, we observe that both of the compounds have the same number and types of CPs in (1 0 0)-plane; there are three non-equivalent BCPs: 1) In2-Ce (b2), 2) In2-M (b3) for M = Co, Rh and 3) In2-In2 (b5). In summery, the results presented in Table 4 and Fig. 8 have already shown that the number and types of CPs are predicted by B3PW91-$\alpha = 0.20$ scheme to be different in the (0 0 1)-plane of these compounds at zero pressure. The fact that $CeMIn_5$ compounds have the same crystal structure but their lattice parameters are different raises a question as to what happen to the number and types of the CPs if the lattice parameters of the two compounds are also the same. To tackle this question, we assumed that lattice parameters of the two compounds were the same and equal to the experimental lattice parameters of $CeRhIn_5$ compound. By this hypothetical assumption, we observed that under this assumption the number and types of CPs of $CeCoIn_5$ remained unchanged within B3PW91-$\alpha = 0.20$. This showed that the different lattice constants could not be the source of the different types and numbers of Co-case compared to Rh-case. Thus, more analysis is needed to settle this issue, as discussed below step by step.

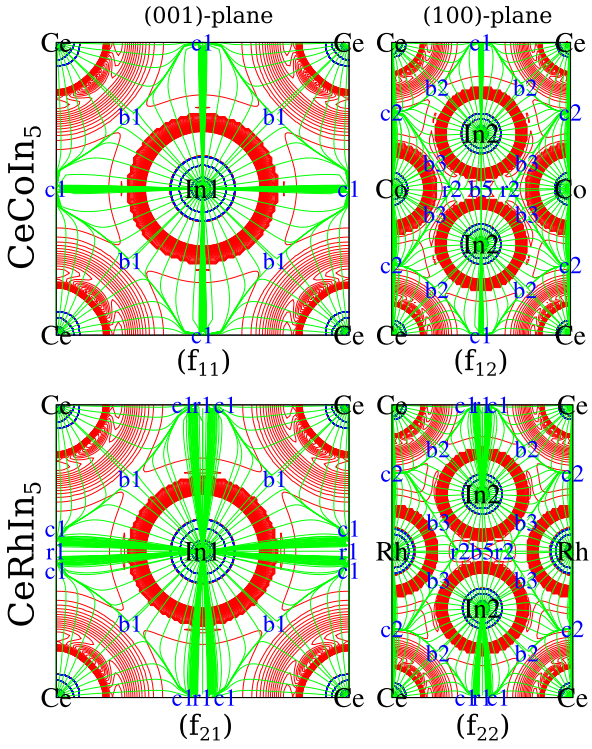

Fig. 8. CPs (blue c, b, r characters), and flux lines generated by $\nabla\rho(\mathbf{r})$ (green curves), as well as $\nabla^2\rho(\mathbf{r})$ (red curves) in the (0 0 1)-plane of (f_{11}) $CeCoIn_5$, (f_{21}) $CeRhIn_5$, and in the (1 0 0)-plane of (f_{12}) $CeCoIn_5$, (f_{22}) $CeRhIn_5$ within B3PW91-$\alpha = 0.20$ functional. The calculations of $CeCoIn_5$ ($CeRhIn_5$) are done in NM (AFM) phase.

The BCP's and their properties are tabulated in Table 5 for $CeCoIn_5$ and $CeRhIn_5$ at zero pressure as well as at pressure of about 4.5 GPa (equivalent to the lattice parameters $a = 4.497$ Å, $c = 7.3612$ Å for $CeCoIn_5$ and $a = 4.577$ Å, $c = 7.4142$ Å for $CeRhIn_5$) within LDA,B3PW91-$\alpha = 0.05$, and B3PW91-$\alpha = 0.20$ exchange-correlation functionals. These values of pressure is calculated within B3PW91-$\alpha = 0.20$ ($\alpha = 0.05$) functional for $CeCoIn_5$ ($CeRhIn_5$) compounds. In this table MULT is the multiplicity of the BCPs in the unit cell, d1 is the distance between BCP and ATOM1, d2 is the distance between BCP and ATOM2, $\widehat{d1 - b - d2}$ is the angle between ATOM1, BCP, and ATOM2 in degree, ρ, and $\nabla^2\rho$ are respectively the values of ECD and its Laplacian evaluated at BCPs. The ρ values at BCPs locations are in agreement with those shown in Figs. 6 and 7. A large value of ρ and a large negative value of $\nabla^2\rho$ at a BCP may provide a covalent bond [64,65]. In contrast, a small value of ρ and a large positive value of $\nabla^2\rho$ at a BCP may provide an ionic bond [64,65]. However, our results show small values for both of the ρ and positive $\nabla^2\rho$ at all BCPs of the considered cases. This can be taken as an indication to the fact that the $CeMIn_5$ may not be considered as purely ionic or purely covalent compounds. Instead, they may be composed of a mixture of ionic and covalent bonds such as LiH and NaH compounds as previously reported by Lixian Zhang and coworkers [64]. The results presented in Table 5 show that the values of ρ and $\nabla^2\rho$ at BCP in (0 0 1)-plane, i.e, b1, in $CeCoIn_5$ are more than those in $CeRhIn_5$ within B3PW91-$\alpha = 0.20$ at zero pressure. Conversely, the $\frac{d1}{d2}$ ratio at b1 in Co-case is lower than that in Rh-case within B3PW91-$\alpha = 0.20$ at zero pressure. The situation is entirely reversed at b2, b3, and b4 compared to b1, however, again as ρ increases $\nabla^2\rho$ also increases and $\frac{d1}{d2}$ decreases. Namely, at b2, b3, and b4 BCPs, ρ and $\nabla^2\rho$ in $CeCoIn_5$ are less than those in $CeRhIn_5$ and conversely the $\frac{d1}{d2}$ ratio in Co-case is higher than that in Rh-case within B3PW91-$\alpha = 0.2$ at zero pressure. Hence, these results show that there would be a direct relation between ρ and $\nabla^2\rho$ and an inverse relation between $\frac{d1}{d2}$ ratio and ρ or

Table 5
BCPs and their properties including MULT as multiplicity of the BCPs in the unit cell; d1 as the distance between BCP and ATOM1; d2 as the distance between BCP and ATOM2; $\widehat{d1-b-d2}$ as the angle between ATOM1, BCP, and ATOM2 in degree; ρ, and $\nabla^2\rho$ as the values of ECD and its Laplacian evaluated at BCPs for $CeCoIn_5$ in non magnetic (NM) phase and $CeRhIn_5$ in antiferromagnetic (AFM) phase at zero pressure as well as P = 4.5 GPa within B3PW91-α = 0.20, B3PW91-α = 0.05 and LDA functionals.

	P(GPa)	BCP	MULT	ATOM1	ATOM2	d1 (bohr)	d2 (bohr)	$\frac{d1}{d2}$	$\widehat{d1-b-d2}$	$\rho\left(\frac{elec}{bohr^3}\times10^{-2}\right)$	$\nabla^2\rho\left(\frac{elec}{bohr^3}\times10^{-2}\right)$
						B3PW91-α = 0.20					
$CeCoIn_5$	0	b1	4	In1	Ce	3.0305	3.0812	0.9835	179.9999	2.4499	3.7056
		b2	8	Ce	In2	3.1027	3.0667	1.0117	176.9619	2.3601	3.5845
		b3	8	In2	Co	2.6491	2.4344	1.0882	177.4774	4.3824	3.9406
		b4	8	In1	In2	3.0974	3.0976	0.9999	169.1438	2.3740	2.0636
		b5	2	In2	In2	2.6746	2.6746	1.0000	179.9999	4.0344	5.6707
	3	b1	4	In1	Ce	2.9688	3.0400	0.9766	179.9999	2.6650	4.2057
		b2	8	In2	Ce	3.0042	3.0614	0.9813	176.9254	2.5742	4.0386
		b3	8	In2	Co	2.6102	2.3879	1.0931	177.4075	4.7220	3.9510
		b4	8	In1	In2	3.0452	3.0449	1.0001	169.2555	2.5700	2.3501
		b5	2	In2	In2	2.6296	2.6296	1.0000	179.9999	4.3543	6.1783
$CeRhIn_5$	0	b1	4	Ce	In1	3.1201	3.1016	1.0060	179.9551	2.1978	3.4465
		b2	8	In2	Ce	3.0477	3.1105	0.9798	177.1020	2.3167	3.7219
		b3	8	Rh	In2	2.6774	2.5481	1.0508	179.3521	4.6949	6.6997
		b4	8	In2	In1	3.0846	3.0919	0.9976	170.7252	2.3840	2.0370
		b5	2	In2	In2	2.8198	2.8198	1.0000	179.9999	3.1882	4.5613
	3	b1	4	In1	Ce	3.0371	3.0790	0.9864	179.9005	2.3891	3.8934
		b2	8	Ce	In2	3.0788	3.0005	1.0261	176.9521	2.4789	4.0896
		b3	8	Rh	In2	2.6264	2.4912	1.0543	179.1213	5.1761	7.1629
		b4	8	In2	In1	3.0444	3.0527	0.9973	170.7070	2.5394	2.2478
		b5	2	In2	In2	2.7359	2.7359	1.0000	179.9999	3.6483	5.4642
						B3PW91-α = 0.05					
$CeCoIn_5$	0	b1	4	In1	Ce	3.0255	3.0862	0.9803	179.9999	2.4740	3.6459
		b2	8	Ce	In2	3.1000	3.0691	1.0100	177.2146	2.3572	3.5743
		b3	8	Co	In2	2.4350	2.6485	0.9194	177.5385	4.3790	3.9651
		b4	8	In1	In2	3.0971	3.0991	0.9994	168.9187	2.3743	2.0628
		b5	2	In2	In2	2.6746	2.6746	1.0000	179.9999	4.0299	5.6891
	3	b1	4	In1	Ce	2.9650	3.0437	0.9741	179.9999	2.6756	4.1771
		b2	8	Ce	In2	3.0575	3.0078	1.0165	177.1550	2.5513	4.0757
		b3	8	In2	Co	2.6094	2.3884	1.0925	177.5253	4.7184	3.9799
		b4	8	In1	In2	3.0448	3.0460	0.9996	169.1373	2.5730	2.3401
		b5	2	In2	In2	2.6296	2.6296	1.0000	179.9999	4.3463	6.2070
$CeRhIn_5$	0	b1	4	Ce	In1	3.1242	3.0974	1.0087	179.8220	2.2285	3.3540
		b2	8	In2	Ce	3.0682	3.1157	0.9847	177.0779	2.3099	3.4987
		b3	8	In2	Rh	2.5381	2.6677	0.9514	179.1238	4.7821	6.7826
		b4	8	In1	In2	3.1051	3.0999	1.0017	170.1093	2.3411	1.9835
		b5	2	In2	In2	2.7831	2.7831	1.0000	179.9999	3.3679	4.9116
	3	b1	4	In1	Ce	3.0334	3.0827	0.9840	179.7461	2.4257	3.8215
		b2	8	Ce	In2	3.0723	3.0066	1.0219	177.1871	2.5186	3.9536
		b3	8	In2	Rh	2.4916	2.6260	0.9488	179.1229	5.1784	7.1463
		b4	8	In2	In1	3.0471	3.0523	0.9983	170.1956	2.5353	2.2643
		b5	2	In2	In2	2.7359	2.7359	1.0000	179.9999	3.6489	5.4695
						LDA					
$CeCoIn_5$	0	b1	4	In1	Ce	3.0250	3.0867	0.9800	179.9999	2.4595	3.7380
		b2	8	Ce	In2	3.0983	3.0706	1.0090	177.3358	2.3306	3.6814
		b3	8	Co	In2	2.4345	2.6487	0.9191	177.7871	4.3824	4.1410
		b4	8	In1	In2	3.0955	3.0984	0.9991	169.3589	2.3625	2.1527
		b5	2	In2	In2	2.6746	2.6746	1.0000	179.9999	4.0269	5.8875
	3	b1	4	In1	Ce	2.9649	3.0439	0.9740	179.9999	2.6713	4.2536
		b2	8	Ce	In2	3.0569	3.0083	1.0161	177.2635	2.5404	4.1570
		b3	8	In2	Co	2.6099	2.3878	1.0930	177.7255	4.7251	4.1584
		b4	8	In1	In2	3.0436	3.0454	0.9994	169.4964	2.5595	2.4469
		b5	2	In2	In2	2.6296	2.6296	1.0000	179.9999	4.3489	6.4160
$CeRhIn_5$	0	b1	4	Ce	In1	3.1315	3.0900	1.0134	179.9241	2.2493	3.3821
		b2	8	In2	Ce	3.0773	3.1063	0.9907	177.2786	2.2943	3.5758
		b3	8	In2	Rh	2.5407	2.6651	0.9533	179.1670	4.7991	6.9363
		b4	8	In2	In1	3.1035	3.1014	1.0007	170.1261	2.3262	2.0831
		b5	2	In2	In2	2.7831	2.7831	1.0000	179.9999	3.3653	5.0721
	3	b1	4	Ce	In1	3.0881	3.0280	1.0199	179.9508	2.4452	3.8569
		b2	8	In2	Ce	3.0146	3.0642	0.9838	177.2553	2.5042	4.0420
		b3	8	In2	Rh	2.4944	2.6232	0.9509	179.1526	5.1982	7.3137
		b4	8	In2	In1	3.0504	3.0487	1.0006	170.2482	2.5215	2.3740
		b5	2	In2	In2	2.7359	2.7359	1.0000	179.9999	3.6485	5.6468

Table 6
Directionality represented by tanα and tanβ accompanied by ellipticity ϵ of bonds of $CeCoIn_5$ in nonmagnetic (NM) phase and $CeRhIn_5$ in antiferromagnetic (AFM) phase at zero pressure as well as P = 4.5 GPa calculated within B3PW91-α = 0.20, B3PW91-α = 0.05, and LDA functionals.

	B3PW91-α = 0.20							
	$CeCoIn_5$				$CeRhIn_5$			
P (GPa)	BCP	tanα	tanβ	ϵ	BCP	tanα	tanβ	ϵ
0	b1	0.43	0.40	0.18	b1	0.41	0.38	0.17
	b2	0.42	0.40	0.10	b2	0.42	0.41	0.04
	b3	0.54	0.50	0.16	b3	0.49	0.47	0.09
	b4	0.50	0.42	0.42	b4	0.51	0.43	0.36
	b5	0.53	0.36	1.19	b5	0.53	0.24	4.00
4.5	b1	0.43	0.39	0.17	b1	0.41	0.38	0.16
	b2	0.42	0.40	0.09	b2	0.42	0.41	0.04
	b3	0.55	0.51	0.16	b3	0.53	0.27	2.95
	b4	0.50	0.42	0.41	b4	0.5	0.43	0.36
	b5	0.53	0.36	1.16	b5	0.53	0.27	2.95
	B3PW91-α = 0.05							
	$CeCoIn_5$				$CeRhIn_5$			
P (GPa)	BCP	tanα	tanβ	ϵ	BCP	tanα	tanβ	ϵ
0	b1	0.43	0.41	0.11	b1	0.42	0.39	0.17
	b2	0.42	0.41	0.04	b2	0.42	0.42	0.03
	b3	0.54	0.50	0.16	b3	0.49	0.47	0.09
	b4	0.50	0.42	0.40	b4	0.42	0.42	0.03
	b5	0.53	0.36	1.19	b5	0.53	0.26	3.06
4.5	b1	0.43	0.41	0.10	b1	0.42	0.39	0.17
	b2	0.41	0.41	0.03	b2	0.42	0.42	0.03
	b3	0.55	0.51	0.16	b3	0.5	0.48	0.09
	b4	0.49	0.42	0.38	b4	0.5	0.43	0.38
	b5	0.53	0.36	1.16	b5	0.53	0.27	2.97
	LDA							
	$CeCoIn_5$				$CeRhIn_5$			
P (GPa)	BCP	tanα	tanβ	ϵ	BCP	tanα	tanβ	ϵ
0	b1	0.43	0.41	0.08	b1	0.42	0.4	0.13
	b2	0.41	0.41	0.02	b2	0.42	0.41	0.02
	b3	0.54	0.5	0.15	b3	0.49	0.47	0.09
	b4	0.49	0.42	0.36	b4	0.5	0.43	0.36
	b5	0.53	0.36	1.13	b5	0.53	0.27	2.85
4.5	b1	0.43	0.41	0.08	b1	0.42	0.39	0.13
	b2	0.41	0.41	0.02	b2	0.42	0.41	0.03
	b3	0.55	0.51	0.15	b3	0.49	0.47	0.09
	b4	0.49	0.42	0.36	b4	0.49	0.42	0.36
	b5	0.53	0.37	1.10	b5	0.53	0.27	2.76

$\nabla^2\rho$ at these BCPs. The above discussion based on the results presented in Table 5 not only supports our last discussion on the number and types of the CPs concluded from Table 4, but also shows that (in addition to the number and types of CPs) ρ, $\nabla^2\rho$, and $\frac{d1}{d2}$ of the compounds under question also differ from each other at zero pressure. We below present more topological evidences in this respect at zero pressure.

Stability of a bond can be quantified by the directionality which is defined by two components: [66,34]

$$\tan\alpha = \sqrt{\frac{\lambda_\perp}{\lambda_\parallel}}, \quad \tan\beta = \sqrt{\frac{\lambda'_\perp}{\lambda_\parallel}}, \tag{3}$$

where α and β angles represent the extreme angles of the elliptic cone constructed by the Hessian of charge density at the BCP and surrounding the bond path. The $\lambda_\parallel$ is the positive eigenvalue of ECD Hessian matrix at the given BCP and represents the principal curvature along the bond path. The $\lambda_\perp$ and $\lambda'_\perp$ ($|\lambda_\perp| \geqslant |\lambda'_\perp|$) are two negative eigenvalues of ECD Hessian matrix at the given BCP and represent the principal curvatures perpendicular to the bond path. Larger values of directionality means that the bond is further from the topological instability. The directionality of bonds of $CeMIn_5$ (M = Co, Rh) compounds are tabulated in Table 6. In this table ellipticity (ϵ) of BCPs are also represented. The ellipticity of a bond provides the measure of extent to which charge is accumulated in the plane constructed by the eigenvectors with negative eigenvalues and is defined as: [35]

$$\epsilon = \frac{|\lambda_\perp|}{|\lambda'_\perp|} - 1; \qquad \left|\lambda_\perp\right| > \left|\lambda'_\perp\right|. \tag{4}$$

Bonds with $\epsilon = 0$ have cylindrical symmetry. Thus, this quantity shows the deviation from the cylindrical symmetry. As Table 6 shows, tanα and tanβ of b1 in Co-case are slightly more than those of Rh-case at zero pressure. This means that the b1 in $CeCoIn_5$ is more stable than that in $CeRhIn_5$ at zero pressure. This result can be seen for the b3 and b5, as well. Conversely, the b2 and b4 in $CeRhIn_5$ are more stable than those in $CeCoIn_5$ at zero pressure. This table shows that the ellipticity values of b1 and b2 for both cases are tiny and thereby negligible. But, more precisely, one observes that the ϵ values at b1 and b2 in Co-case are slightly more than that in Rh-case. This shows that the deviation from cylindrical symmetry of b1 and b2 in Co-case are more than that in Rh-case. This is similar to what we see for b3 and b4 BCPs; Co-case is more deviated than Rh-case from the cylindrical symmetry. In the case of b5, the ϵ values are very large for both of the compounds and it is almost 3 times larger for Rh-case than that for Co-case. This demonstrates that both of the cases are highly deviated from the cylindrical symmetry at b5 BCP and the deviation of the Rh-case is three times larger than that of Co-case. The above discussion inspired from Table 6 again confirms our last statements inferred from Fig. 8, Tables 4 and 5 that (in addition to the number and types, ρ, $\nabla^2\rho$, and $\frac{d1}{d2}$) directionality, ellipticity, and stability of the compounds are also different at zero pressure. Let us below continue by shifting our focus on the effects of pressure.

As shown in Table 5, applying pressure on $CeRhIn_5$ increases ρ and $\nabla^2\rho$ at all of the bonds. Thus, pressure makes the ρ and $\nabla^2\rho$ at b1, b2 and b5 (b3, b4) more similar to (different from) those of $CeCoIn_5$. Applying pressure also makes the $\frac{d1}{d2}$ ratio of b1 very similar to that of $CeCoIn_5$. More precisely, applying pressure on the Rh-case causes the $\frac{d1}{d2}$ at b3 CP to become more different from those of Co-case, which is not the case at b2 and b4 CPs. The $\frac{d1}{d2}$ of b5 in two cases is similar and it is equal to 1.000. Applying pressure on Rh-case does not change this ratio and it remains equal to 1.000 in Rh-case under pressure. So, pressure can make the BCP properties of Rh-case in (0 0 1)-plane more similar to that of Co-case. However, pressure cannot still change the number and types of CPs of $CeRhIn_5$ within the localized B3PW91-α = 0.20. Furthermore, as shown in Table 6, the stability and ellipticity of $CeRhIn_5$ bonds cannot be also changed by applying pressure within B3PW91-α = 0.20 functional.

Shishido and coworkers [37,38] using dHvA experiments have shown that the degree of 4f-electron localization has been decreased by imposing pressure on $CeRhIn_5$. These interesting experimental evidences motivated us to investigate the effects of 4f-electrons localization degree on the TECD of $CeMIn_5$ (M = Co, Rh), as well. Consequently in addition to the highly localized B3PW91-α = 0.20 functional, we considered B3PW91-α = 0.05 and LDA and recalculated the TECD of these compounds using these lower localized functionals compered to B3PW91-α = 0.20 to evaluate what happen to the TECD after reducing the degree of 4f-electrons localization. The degree of 4f-electrons localization is considered to be much lower by LDA functional compared to the hybrid B3PW91-α = 0.20 and B3PW91-α = 0.05 functionals. The B3PW91-α = 0.05 and LDA calculations are performed at zero experimental pressure by employing experimental lattice constants. As Table 4 shows, the numbers and types of CPs within B3PW91-α = 0.05 are the same as those of B3PW91-α = 0.20 for both cases under study.

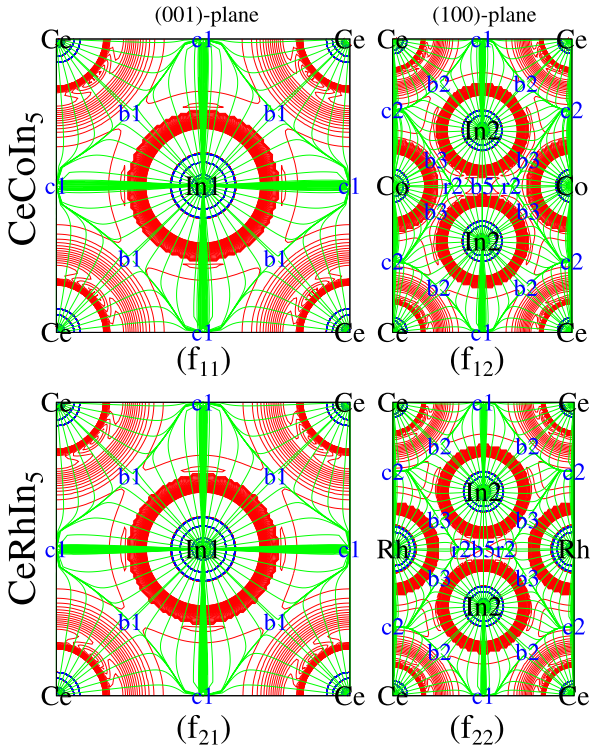

Fig. 9. CPs (blue c, b, r charchters), and flux lines generated by $\nabla\rho(\mathbf{r})$ (green curves), as well as $\nabla^2\rho(\mathbf{r})$ (red curves) in the (0 0 1)-plane of (f_{11}) $CeCoIn_5$, (f_{21}) $CeRhIn_5$, and in the (100)-plane of (f_{12}) $CeCoIn_5$, (f_{22}) $CeRhIn_5$, within LDA functional. The calculations of $CeCoIn_5$ ($CeRhIn_5$) are done in NM (AFM) phase.

But the situation is completely different with the LDA functional. The CPs of the compounds as calculated by LDA are shown for (0 0 1)-plane in the left panel, and for (100)-plane in the right panel of Fig. 9. The number and types of $CeMIn_5$ (M = Co, Rh) CPs calculated within LDA functional are reported in Table 4. As this table shows, the number and types of $CeCoIn_5$ CPs obtained by LDA are the same as those obtained by B3PW91-α = 0.20 and B3PW91-α = 0.05. This result can be also seen by comparing Figs. 9(f_{1j}) with Figs. 8f_{1j}) (j = 1,2) for both (0 0 1) and (1 0 0) planes. On the contrary, the number and types of $CeRhIn_5$ CPs within LDA are different from those of B3PW91-α = 0.20 and B3PW91-α = 0.05, see Table 4, which can be also seen by comparing Figs. 9(f_{2j}) with Figs. 8 (f_{2j}) (j = 1,2) for both (0 0 1) and (1 0 0) planes. Similarity of LDA and B3PW91-α = 0.20 results for the case of $CeCoIn_5$ indicates that 4f-electrons in this case are itinerant and thereby can be well described by the band-like LDA functional so that the hybrid functional is not necessary to be used, i.e., B3PW91-α = 0.05 and B3PW91-α = 0.20 do not improve the LDA results. On the contrary, 4f-electrons in the $CeRhIn_5$ are so localized that the itinerant LDA functional fails to well describe them at zero pressure and thereby B3PW91-α = 0.20 is more suitable for this purpose. These results are in agreement with previous theoretical calculations [39]. Interestingly, we observe that the number and types of equivalent CPs calculated by LDA for $CeRhIn_5$ are now the twice as many as those calculated by B3PW91 with α = 0.20 for $CeCoIn_5$. As Fig. 9(f_{21}) shows, the c1 in (0 0 1)-plane stays exactly on the middle of the line connecting two Ce atoms within LDA for $CeRhIn_5$, which is the same as that we see within LDA or B3PW91-α = 0.20 functionals for $CeCoIn_5$. Therefore, in the (0 0 1)-plane of $CeRhIn_5$ within the LDA approximation only one c1 is seen between Ce atoms, see Fig. 9(f_{21}). In other words, reducing the degree of 4f-electrons localization in $CeRhIn_5$ makes the number and types of its CPs the same as those of $CeCoIn_5$ in the (0 0 1)-plane. Comparison of Fig. 9(f_{22}) with Fig. 8(f_{22}) shows that the TECD of $CeRhIn_5$ in (100)-plane within LDA is the same as B3PW91-α = 0.20. The properties of $CeMIn_5$ BCPs within LDA are represented in Table 5. As the latter table shows, the ρ and $\nabla^2\rho$ of BCPs within LDA are different from those of $CeCoIn_5$. The directionalities of $CeRhIn_5$ bonds within LDA are also very similar to that of B3PW91-α = 0.20 and B3PW91-α = 0.05. Thus, in summary we can say that although reducing the 4f-electrons localization can make the number and types of Rh-case CPs similar to those of Co-case, it alone cannot force $CeRhIn_5$ to behave as $CeCoIn_5$ concerning the BCP properties.

Now time seems apt to put the effects of pressure together with the effects of reducing 4f-electrons localization degree, as discussed above. From the above discussions on the pressure and localization effects one can anticipate that a combination of pressure and reduction of 4f-electrons localization can be the key idea for solving the problem to make the TECD of $CeRhIn_5$ very similar to that of $CeCoIn_5$ in (0 0 1)-plane considering both BCPs properties and number and types of CPs. Our results confirm this anticipation. As shown in Table 5, BCP properties of the $CeRhIn_5$ at P~ 4.5 GPa within LDA are very similar to those of $CeCoIn_5$ within LDA and B3PW91-α = 0.20. Furthermore, the number and types of pressed Rh-case equivalent CPs within LDA are twice as many as $CeCoIn_5$ within LDA and B3PW91-α = 0.20. These results, in accordance with experiments [8,16,13], reveal that pressure can cause the TECD features of $CeRhIn_5$ to become very similar to those of the $CeCoIn_5$ in (0 0 1)-plane, if the degree of 4f-electrons localization is also simultaneously reduced, e.g., simply by employing LDA functional.

Recently, it is experimentally reported [8,41,17,16,42,43] that Sn doping on $CeRhIn_5$ and $CeCoIn_5$ would decrease P_c of the former case and T_c of the latter case. These important observations motivated us to calculate the effects of Sn doping at In site on the TECD of $CeRhIn_5$ and $CeCoIn_5$, as well. To this end, we calculated the TECDs of $CeMIn_{4.5}Sn_{0.5}$ for M = Co (Rh) in NM (AFM) phase within B3PW91-α = 0.20. The number and types of CPs in 1 × 2 × 1 cell of these cases are reported in Table 7. This table clearly demonstrates the fulfillment of the Morse condition for the CPs of the Sn-doped cases.

The CPs of the doped compounds in the (0 0 1)-plane are shown in Fig. 10. In this figure we label CPs of the doped cases with capital letter to be distinguished from those of the pure cases. Comparison of Fig. 10(f_{11}) with Figs. 8(f_{i1}) (i = 1,2) shows that the number and types of Sn-doped of $CeCoIn_5$ are similar to pure $CeCoIn_5$. Namely, the same as pure Co-case there are one CCP between Ce atoms in the Sn-doped of the Co-case. However, comparison of Fig. 10(f_{12}) with Figs. 8(f_{i1}) (i = 1,2) shows that the number and types of Sn-doped of $CeRhIn_5$ are more similar to those of pure $CeRhIn_5$ along the [001] (Fig. 8(f_{21})), and more similar to pure $CeCoIn_5$ along the [100] direction (Fig. 8(f_{11})). These results show that Sn doping in $CeRhIn_5$ can make the number and types of CPs in (0 0 1)-plane some what similar to pure case of $CeCoIn_5$. According to these results, Sn doping decreases the degree of 4f-electron localization in $CeRhIn_5$ case. This effect of Sn was reported for the $CeIn_3$ case too [67]. In contrast to hydrostatic pressure, our results also show that Sn doping decreases ρ at BCP between In1 and Ce, i.e., B1, as well as its directionality in both Co- and Rh-cases. Similar result is reached for the $\nabla^2\rho$ of B1 in Rh-case. Hence, Sn doping causes the BCP properties of Rh-case (Co-case) in (0 0 1)-plane to be far from (more similar to) the pure case of $CeCoIn_5$ ($CeRhIn_5$). This shows that the effects of Sn doping depends on its hosts so that it can play a dual role in these compounds. Namely, the above results, consistent with the

Table 7
Number and types of non-equivalent CPs for $CeMIn_{4.5}Sn_{0.5}$ (M = Co, Rh) compounds calculated within B3PW91-α = 0.20 functional. The calculations of $CeCoIn_{4.5}Sn_{0.5}$ ($CeRhIn_{4.5}Sn_{0.5}$) are done in NM (AFM) phase. The numbers in parentheses represent the number of equivalent CPs.

	NCP	BCP	RCP	CCP
$CeCoIn_{4.5}Sn_{0.5}$	10(14)	26(60)	22(72)	12(26)
$CeRhIn_{4.5}Sn_{0.5}$	10(14)	26(60)	25(75)	13(29)

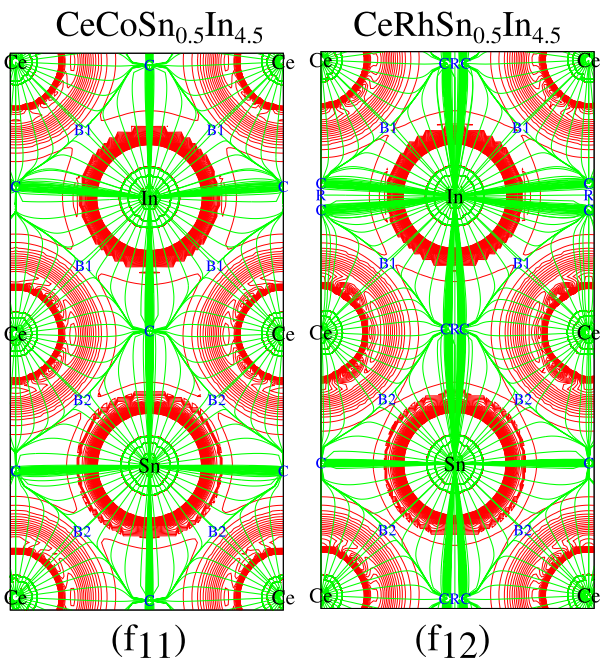

Fig. 10. CPs (blue c, b, r charchters), and flux lines generated by $\nabla\rho(\mathbf{r})$ (green curves), as well as $\nabla^2\rho(\mathbf{r})$ (red curves) in the (0 0 1)-plane of (f_{11}) $CeCoIn_{4.5}Sn_{0.5}$, (f_{12}) $CeRhIn_{4.5}Sn_{0.5}$ within B3PW91-$\alpha = 0.20$ functional. The calculations of $CeCoIn_5$ ($CeRhIn_5$) are done in NM (AFM) phase.

experiments [8,41,17,16,42,43], clearly show that the role of Sn impurity is reversed when it is doped into $CeRhIn_5$; it causes $CeRhIn_5$ to deviate from its pure case to behave somewhat like $CeCoIn_5$. On the other hand, Sn doping causes $CeCoIn_5$ to deviate from its pure case to behave like $CeRhIn_5$.

6. Conclusions

In this work, structural properties and electronic structures, including band structures, densities of states (DOSs), and electron charge densities (ECDs), as well as topology of ECDs (TECDs) are calculated for the isostructural $CeCoIn_5$ and $CeRhIn_5$ compounds by a combination of density functional theory (DFT) and quantum theory of atoms in molecules (QTAIM) using a variety of exchange–correlation functionals. Investigation of DOSs and band structures reveals that decreasing the degree of localization for the 4f-Ce electrons considerably affects the electronic structures of the compounds under study. The effects of applying pressure on DOSs and band structures reveal that although decreasing the degree of localization for 4f-Ce electrons considerably affects the electronic structures of compounds, the pressure effects are negligible compared to the effects of degree of localization. From our DFT + QTAIM calculations, the following results are obtained: The TECD of these compounds are found to be different in number and types of critical points (CPs) in the edges of the (0 0 1)-plane at zero pressure. The 4f-electrons of the Co-case lie in the low localized regime so that they can be well described by the band-like LDA functional, while this is not the case for $CeRhIn_5$. The effects of 4f-electrons localization on the TECD of the other planes are almost negligible. The above differences are vanished by decreasing the degree of 4f-electrons localization in $CeRhIn_5$, i.e., the number and types of CPs in $CeRhIn_5$ within the low localized LDA functional are found to be the same as $CeCoIn_5$. In addition to the above differences, it is also shown that there are many other differences between bond critical points properties of these compounds which can be vanished in (0 0 1)-plane by applying pressure on the $CeRhIn_5$ case. Namely, our results show that applying pressure on the Rh-case and simultaneously decreasing its 4f-electrons localization can make the TECD of $CeRhIn_5$ very similar to that of $CeCoIn_5$. Furthermore, the effects of Sn doping are investigated on the TECD of these compounds. Our results show that the Sn doping can make the TECD of $CeRhIn_5$ ($CeCoIn_5$) somewhat similar to that of pure $CeCoIn_5$ ($CeRhIn_5$). Our results also show that Sn doping in these compounds plays a dual role depending on its hosts. All the DFT + QTAIM results presented in this work are found to be consistent with the reliable experimental data.

CRediT authorship contribution statement

M. Yazdani-Kachoei: Conceptualization, Data curation, Formal analysis, Investigation, Methodology, Validation, Visualization, Writing - original draft. **S. Jalali-Asadabadi:** Conceptualization, Data curation, Formal analysis, Funding acquisition, Investigation, Methodology, Project administration, Resources, Software, Supervision, Validation, Visualization, Writing - review & editing. **Negar Arianmehr:** Conceptualization, Data curation, Formal analysis, Methodology.

References

[1] B.B. Zhou, S. Misra, E.H. da Silva Neto, P. Aynajian, R.E. Baumbach, J.D. Thompson, E.D. Bauer, A. Yazdani, Visualizing nodal heavy fermion superconductivity in $CeCoIn_5$, Nat. Phys. 9 (2013) 474–479.
[2] T. Park, H. Lee, I. Martin, X. Lu, V.A. Sidorov, K. Gofryk, F. Ronning, E.D. Bauer, J.D. Thompson, Textured superconducting phase in the heavy fermion $CeRhIn_5$, Phys. Rev. Lett. 108 (2012) 077003 URLhttp://link.aps.org/doi/10.1103/PhysRevLett.108.077003.
[3] S. Qimiao, F. Steglich, Heavy fermions and quantum phase transitions, Science 329 (5996) (2010) 1161–1166 URLhttp://www.sciencemag.org/content/329/5996/1161.abstract.
[4] S. Raymond, J. Buhot, E. Ressouche, F. Bourdarot, G. Knebel, G. Lapertot, Switching of the magnetic order in $CeRhIn_{5-x}Sn_x$ in the vicinity of its quantum critical point, Phys. Rev. B 90 (2014) 014423 URLhttp://link.aps.org/doi/10.1103/PhysRevB.90.014423.
[5] M.R. Norman, The challenge of unconventional superconductivity, Science 332 (6026) (2011) 196–200 URLhttp://www.sciencemag.org/content/332/6026/196.abstract.
[6] D.P.P. Monthoux, G.G. Lonzarich, Superconductivity without phonons, Nature 450 (7173) (2007) 1177–1183.
[7] T. Park, F. Ronning, H.Q. Yuan, M.B. Salamon, R. Movshovich, J.L. Sarrao, J.D. Thompson, Hidden magnetism and quantum criticality in the heavy fermion superconductor $CeRhIn_5$, Nature 440 (7080) (2006) 65–68.
[8] S. Seo, E. Park, E.D. Bauer, F. Ronning, J.N. Kim, J.H. Shim, J.D. Thompson, T. Park, Controlling superconductivity by tunable quantum critical point, Nat. Commun. 6 (2015) 6433.
[9] V.A. Sidorov, X. Lu, T. Park, H. Lee, P.H. Tobash, R.E. Baumbach, F. Ronning, E.D. Bauer, J.D. Thompson, Pressure phase diagram and quantum criticality of $CePt_2In_7$ single crystals, Phys. Rev. B 88 (2013) 020503 URLhttp://link.aps.org/doi/10.1103/PhysRevB.88.020503.
[10] J.L. Sarrao, J.D. Thompson, Superconductivity in Cerium- and Plutonium-Based '115' materials, J. Phys. Soc. Jpn. 76 (5) (2007) 051013, https://doi.org/10.1143/JPSJ.76.051013.
[11] J.D. Thompson, Z. Fisk, Progress in heavy-fermion superconductivity: Ce-115 and related materials, J. Phys. Soc. Jpn. 81 (1) (2012) 011002, https://doi.org/10.1143/JPSJ.81.011002.
[12] C. Petrovic, R. Movshovich, M. Jaime, P.G. Pagliuso, M.F. Hundley, J.L. Sarrao, Z. Fisk, J.D. Thompson, A new heavy-fermion superconductor $CeIrIn_5$: a relative of the cuprates? EPL (Europhysics Letters) 53 (3) (2001) 354.
[13] H. Hegger, C. Petrovic, E.G. Moshopoulou, M.F. Hundley, J.L. Sarrao, Z. Fisk, J.D. Thompson, Pressure-induced superconductivity in Quasi-2D $CeRhIn_5$, Phys. Rev. Lett. 84 (2000) 4986–4989 URLhttp://link.aps.org/doi/10.1103/PhysRevLett.84.4986.
[14] F.P. Mena, D. van der Marel, J.L. Sarrao, Optical conductivity of $CeMIn_5$ (M = Co, Rh, Ir), Phys. Rev. B 72 (2005) 045119 URLhttp://link.aps.org/doi/10.1103/PhysRevB.72.045119.
[15] E.J. Singley, D.N. Basov, E.D. Bauer, M.B. Maple, Optical conductivity of the heavy fermion superconductor $CeCoIn_5$, Phys. Rev. B 65 (2002) 161101 URLhttp://link.aps.org/doi/10.1103/PhysRevB.65.161101.
[16] G. Knebel, J. Buhot, D. Aoki, G. Lapertot, S. Raymond, E. Ressouche, J. Flouquet, Antiferromagnetism and superconductivity in $CeRhIn_5$, J. Phys. Soc. Japan 80 (Suppl.A) (2011) SA001.10.1143/JPSJS.80SA.SA001.
[17] K. Gofryk, F. Ronning, J.-X. Zhu, M.N. Ou, P.H. Tobash, S.S. Stoyko, X. Lu, A. Mar, T. Park, E.D. Bauer, J.D. Thompson, Z. Fisk, Electronic tuning and uniform superconductivity in $CeCoIn_5$, Phys. Rev. Lett. 109 (2012) 186402 URLhttp://link.aps.org/doi/10.1103/PhysRevLett.109.186402.
[18] T. Björkman, R. Lizárraga, F. Bultmark, O. Eriksson, J.M. Wills, A. Bergman, P.H. Andersson, L. Nordström, Theoretical studies of the incommensurate magnetic structure of a heavy fermion system:$CeRhIn_5$, Phys. Rev. B 81 (2010) 094433 URLhttp://link.aps.org/doi/10.1103/PhysRevB.81.094433.
[19] J. Rusz, P.M. Oppeneer, N.J. Curro, R.R. Urbano, B.-L. Young, S. Lebègue, P.G. Pagliuso, L.D. Pham, E.D. Bauer, J.L. Sarrao, Z. Fisk, Probing the electronic structure of pure and doped $CeMIn_5$ (M = Co,Rh,Ir) crystals with nuclear quadrupolar resonance, Phys. Rev. B 77 (2008) 245124 URLhttp://link.aps.org/doi/10.

1103/PhysRevB.77.245124.
[20] M. Gamża, A. Ślebarski, J. Deniszczyk, Electronic structure of $Ce_nM_mIn_{2m+3n}$, where n = 1, 2; m = 0, 1;M = Co, Rh or Ir: experiment and calculations, J. Phys.: Condens. Matter 20 (11) (2008) 115202 URLhttp://stacks.iop.org/0953-8984/20/i=11/a=115202.
[21] S. Elgazzar, I. Opahle, R. Hayn, P.M. Oppeneer, Calculated de Haas-van Alphen quantities of $CeMIn_5$(M = Co, Rh, and Ir) compounds, Phys. Rev. B 69 (2004) 214510 URLhttp://link.aps.org/doi/10.1103/PhysRevB.69.214510.
[22] D. Hall, E.C. Palm, T.P. Murphy, S.W. Tozer, C. Petrovic, E. Miller-Ricci, L. Peabody, C.Q.H. Li, U. Alver, R.G. Goodrich, J.L. Sarrao, P.G. Pagliuso, J.M. Wills, Z. Fisk, Electronic structure of $CeRhIn_5$: de Haas-van Alphen and energy band calculations, Phys. Rev. B 64 (2001) 064506 URLhttp://link.aps.org/doi/10.1103/PhysRevB.64.064506.
[23] D. Moore, T. Durakiewicz, J. Joyce, A. Arko, L. Morales, J. Sarrao, P. Pagliuso, J. Wills, C. Olson, The electronic structure of $CeRhIn_5$ and LaRhIn5 from ARPES, Physica B 312 (2002) 134–135 the International Conference on Strongly Correlated Electron Systems.http://www.sciencedirect.com/science/article/pii/S0921452601011887.
[24] A. Llobet, J.S. Gardner, E.G. Moshopoulou, J.-M. Mignot, M. Nicklas, W. Bao, N.O. Moreno, P.G. Pagliuso, I.N. Goncharenko, J.L. Sarrao, J.D. Thompson, Magnetic structure of $CeRhIn_5$ as a function of pressure and temperature, Phys. Rev. B 69 (2004) 024403 URLhttp://link.aps.org/doi/10.1103/PhysRevB.69.024403.
[25] S. Majumdar, G. Balakrishnan, M.R. Lees, D.M. Paul, G.J. McIntyre, Pressure-induced change in the magnetic modulation of $CeRhIn_5$, Phys. Rev. B 66 (2002) 212502 URLhttp://link.aps.org/doi/10.1103/PhysRevB.66.212502.
[26] R.T. Macaluso, J. Sarrao, P. Pagliuso, N. Moreno, R. Goodrich, D. Browne, F.R. Fronczek, J.Y. Chan, Crystal growth and structure determination of $LaMIn_5$ (M = Co, Rh, Ir), J. Solid State Chem. 166 (1) (2002) 245–250 URLhttp://www.sciencedirect.com/science/article/pii/S0022459602995976.
[27] E. Moshopoulou, Z. Fisk, J. Sarrao, J. Thompson, Crystal growth and intergrowth structure of the new heavy fermion materials $CeIrIn_5$ and $CeRhIn_5$, J. Solid State Chem. 158 (1) (2001) 25–33 URLhttp://www.sciencedirect.com/science/article/pii/S0022459600990522.
[28] E. Moshopoulou, J. Sarrao, P. Pagliuso, N. Moreno, J. Thompson, Z. Fisk, R. Ibberson, Comparison of the crystal structure of the heavy-fermion materials $CeCoIn_5$, $CeRhIn_5$ and $CeIrIn_5$, Appl. Phys. A 74 (1) (2002) s895–s897, https://doi.org/10.1007/s003390201673.
[29] M. Forker, P.R.J. Silva, J.T.P.D. Cavalcante, F.H.M. Cavalcante, S.M. Ramos, H. Saitovitch, E. Baggio-Saitovitch, R. Alonso, M. Taylor, L.A. Errico, Electric field gradients of $CeMIn_5$ (M = Co, Rh, Ir) heavy-fermion systems studied by perturbed angular correlations and ab initio electronic structure calculations, Phys. Rev. B 87 (2013) 155132 URLhttp://link.aps.org/doi/10.1103/PhysRevB.87.155132.
[30] N. Curro, R. Urbano, B.-L. Young, Probing the magnetism in the heavy fermion systems by NMR, Physica B 403 (5–9) (2008) 1010–1012 proceedings of the International Conference on Strongly Correlated Electron Systems.http://www.sciencedirect.com/science/article/pii/S0921452607010253.
[31] N.J. Curro, Hyperfine interactions in the heavy fermion $CeMIn_5$ systems, New J. Phys. 8 (9) (2006) 173 URLhttp://stacks.iop.org/1367-2630/8/i=9/a=173.
[32] T. Stürzer, G. Derondeau, D. Johrendt, Role of different negatively charged layers in $Ca_{10}(FeAs)_{10}(Pt_4As_8)$ and superconductivity at 30 k in electron-doped $(Ca_{0.8}La_{0.2})_{10}(FeAs)_{10}(Pt_3As_8)$, Phys. Rev. B 86 (2012) 060516 URLhttp://link.aps.org/doi/10.1103/PhysRevB.86.060516.
[33] M.E. Eberhart, T.E. Jones, Cauchy pressure and the generalized bonding model for nonmagnetic bcc transition metals, Phys. Rev. B 86 (2012) 134106 URLhttp://link.aps.org/doi/10.1103/PhysRevB.86.134106.
[34] T.E. Jones, M.E. Eberhart, D.P. Clougherty, Topology of the spin-polarized charge density in bcc and fcc iron, Phys. Rev. Lett. 100 (2008) 017208 URLhttp://link.aps.org/doi/10.1103/PhysRevLett.100.017208.
[35] R.F.W. Bader, Atoms in Molecules: A Quantum Theory (International Series of Monographs on Chemistry), Oxford University Press, 1994.
[36] R.F.W. Bader, A quantum theory of molecular structure and its applications, Chem. Rev. 91 (5) (1991) 893–928, https://doi.org/10.1021/cr00005a013.
[37] H. Shishido, R. Settai, H. Harima, Y. Ōnuki, A change of the Fermi surface in $CeRhIn_5$ under pressure, Physica B: Condensed Matter 378 (2006) 92–93, proceedings of the International Conference on Strongly Correlated Electron SystemsSCES 2005Proceedings of the International Conference on Strongly Correlated Electron Systems.http://www.sciencedirect.com/science/article/pii/S0921452606000330.
[38] H. Shishido, R. Settai, H. Harima, Y. Ōnuki, A drastic change of the Fermi surface at a critical pressure in $CeRhIn_5$: dHvA study under pressure, J. Phys. Soc. Japan 74 (4) (2005) 1103–1106, https://doi.org/10.1143/JPSJ.74.1103.
[39] K. Haule, C.-H. Yee, K. Kim, Dynamical mean-field theory within the full-potential methods: Electronic structure of $CeIrIn_5$, $CeCoIn_5$, and $CeRhIn_5$, Phys. Rev. B 81 (2010) 195107URLhttp://link.aps.org/doi/10.1103/PhysRevB.81.195107.
[40] M. Yazdani-Kachoei, S. Jalali-Asadabadi, I. Ahmad, K. Zarringhalam, Pressure dependency of localization degree in heavy fermion $CeIn_3$: a density functional theory analysis, Sci. Rep. 6 (2016) 31734, https://doi.org/10.1038/srep31734.
[41] T. Shang, R.E. Baumbach, K. Gofryk, F. Ronning, Z.F. Weng, J.L. Zhang, X. Lu, E.D. Bauer, J.D. Thompson, H.Q. Yuan, $CeIrIn_5$: superconductivity on a magnetic instability, Phys. Rev. B 89 (2014) 041101 URLhttp://link.aps.org/doi/10.1103/PhysRevB.89.041101.
[42] L.D. Pham, T. Park, S. Maquilon, J.D. Thompson, Z. Fisk, Reversible tuning of the heavy-fermion ground state in $CeCoIn_5$, Phys. Rev. Lett. 97 (2006) 056404 URLhttp://link.aps.org/doi/10.1103/PhysRevLett.97.056404.
[43] E. Bauer, D. Mixson, F. Ronning, N. Hur, R. Movshovich, J. Thompson, J. Sarrao, M. Hundley, P. Tobash, S. Bobev, Antiferromagnetic quantum critical point in $CeRhIn_{5-x}Sn_x$, Physica B 378 (0) (2006) 142–143 proceedings of the International Conference on Strongly Correlated Electron Systems SCES 2005 Proceedings of the International Conference on Strongly Correlated Electron Systems.http://www.sciencedirect.com/science/article/pii/S0921452606000573.
[44] P. Hohenberg, W. Kohn, Inhomogeneous electron gas, Phys. Rev. 136 (1964) B864–B871 URLhttp://link.aps.org/doi/10.1103/PhysRev.136.B864.
[45] W. Kohn, L.J. Sham, Self-consistent equations including exchange and correlation effects, Phys. Rev. 140 (1965) A1133–A1138 URLhttp://link.aps.org/doi/10.1103/PhysRev.140.A1133.
[46] E. Sjöstedt, L. Nordström, D. Singh, An alternative way of linearizing the augmented plane-wave method, Solid State Commun. 114 (1) (2000) 15–20 URLhttp://www.sciencedirect.com/science/article/pii/S0038109899005773.
[47] G.K.H. Madsen, P. Blaha, K. Schwarz, E. Sjöstedt, L. Nordström, Efficient linearization of the augmented plane-wave method, Phys. Rev. B 64 (2001) 195134 URLhttp://link.aps.org/doi/10.1103/PhysRevB.64.195134.
[48] P. Blaha, K. Schwarz, G.K.H. Madsen, D. Kvasnicka, J. Luitz, WIEN2k: An Augmented Plane Waves plus Local Orbitals Program for Calculating Crystal Properties, Vienna University of Technology, Austria, 2001.
[49] H.J. Monkhorst, J.D. Pack, Special points for brillouin-zone integrations, Phys. Rev. B 13 (1976) 5188–5192 URLhttp://link.aps.org/doi/10.1103/PhysRevB.13.5188.
[50] A.D. Becke, A new mixing of Hartree-Fock and local density functional theories, J. Chem. Phys. 98 (1993) 1372–1377.
[51] P.J. Stephens, F.J. Devlin, C.F. Chabalowski, M.J. Frisch, Ab initio calculation of vibrational absorption and circular dichroism spectra using density functional force fields, J. Phys. Chem. 98 (45) (1994) 11623–11627.
[52] V.I. Anisimov, J. Zaanen, O.K. Andersen, Band theory and mott insulators: Hubbard U instead of stoner I, Phys. Rev. B 44 (1991) 943–954 URLhttp://link.aps.org/doi/10.1103/PhysRevB.44.943.
[53] A.D. Becke, Density-functional exchange-energy approximation with correct asymptotic behavior, Phys. Rev. A 38 (1988) 3098–3100 URLhttp://link.aps.org/doi/10.1103/PhysRevA.38.3098.
[54] J.P. Perdew, J.A. Chevary, S.H. Vosko, K.A. Jackson, M.R. Pederson, D.J. Singh, C. Fiolhais, Atoms, molecules, solids, and surfaces: applications of the generalized gradient approximation for exchange and correlation, Phys. Rev. B 46 (1992) 6671–6687 URLhttp://link.aps.org/doi/10.1103/PhysRevB.46.6671.
[55] A.D. Becke, Density functional thermochemistry. iii. The role of exact exchange, J. Chem. Phys. 98 (1993) 5648–5652, https://doi.org/10.1063/1.464913 URLhttp://scitation.aip.org/content/aip/journal/jcp/98/7/10.1063/1.464913.
[56] A.O. de-la Roza, E.R. Johnson, V. Luaña, Critic2: a program for real-space analysis of quantum chemical interactions in solids, Comput. Phys. Commun. 185 (3) (2014) 1007–1018 URLhttp://www.sciencedirect.com/science/article/pii/S0010465513003718.
[57] A.O. de-la Roza, M. Blanco, A.M. Pendás, V. Luaña, Critic: a new program for the topological analysis of solid-state electron densities, Comput. Phys. Commun. 180 (1) (2009) 157–166 URLhttp://www.sciencedirect.com/science/article/pii/S0010465508002865.
[58] R.S. Kumar, A.L. Cornelius, J.L. Sarrao, Compressibility of $CeMIn_5$and Ce_2MIn_8 (M = Rh, Ir, and Co) compounds, Phys. Rev. B 70 (2004) 214526 URLhttp://link.aps.org/doi/10.1103/PhysRevB.70.214526.
[59] F. Birch, Finite elastic strain of cubic crystals, Phys. Rev. 71 (1947) 809–824 URLhttp://link.aps.org/doi/10.1103/PhysRev.71.809.
[60] A.J. Ochoa-Calle, C.M. Zicovich-Wilson, R. Hernández-Lamoneda, A. Ramírez-Solís, Understanding the ε and ζ high-pressure solid phases of oxygen. Systematic periodic density functional theory studies using localized atomic basis, J. Chem. Theory Comput. 11 (3) (2015) 1195–1205, https://doi.org/10.1021/acs.jctc.5b00017.
[61] A. Ochoa-Calle, C. Zicovich-Wilson, A. Ramírez-Solís, On the raman and infrared vibrational spectra of the studies with localized basis sets, Chem. Phys. Lett. 638 (2015) 82–86 URLhttp://www.sciencedirect.com/science/article/pii/S0009261415006338.
[62] A.J. Ochoa-Calle, C.M. Zicovich-Wilson, A. Ramírez-Solís, Solid oxygen ζphase and its transition from εphase at extremely high pressure: a first-principles analysis, Phys. Rev. B 92 (2015) 085148 URLhttp://link.aps.org/doi/10.1103/PhysRevB.92.085148.
[63] M. Caffarel, E. Giner, A. Scemama, A. Ramírez-Solís, Spin density distribution in open-shell transition metal systems: a comparative post-hartree-fock, density functional theory, and quantum monte carlo study of the $CuCl_2$ molecule, J. Chem. Theory Comput. 10 (12) (2014) 5286–5296, https://doi.org/10.1021/ct5004252.
[64] L. Zhang, F. Ying, W. Wu, P. Hiberty, S. Shaik, Topology of electron charge density for chemical bonds from valence bond theory: a probe of bonding types, Chem. – A Eur. J. 15 (12) (2009) 2979–2989, https://doi.org/10.1002/chem.200802134.
[65] S. Fahad, G. Murtaza, T. Ouahrani, R. Khenata, M. Yousaf, S. Omran, S. Mohammad, Structural, elastic, electronic, bonding, and optical properties of $BeAZ_2$ (A = Si, Ge, Sn; Z = P, As) chalcopyrites, J. Alloy. Compd. 646 (2015) 211–222 URLhttp://www.sciencedirect.com/science/article/pii/S0925838815301444.
[66] M. Eberhart, From topology to geometry, Can. J. Chem. 74 (6) (1996) 1229–1235, https://doi.org/10.1139/v96-138.
[67] E.M. Bittar, C. Adriano, C. Giles, C. Rettori, Z. Fisk, P.G. Pagliuso, Probing the localized to itinerant behavior of the 4f electron in $CeIn_{3-x}Sn_x$ by Gd^{3+} electron spin resonance, Phys. Rev. B 86 (2012) 125108 URLhttp://link.aps.org/doi/10.1103/PhysRevB.86.125108.